



JAEA-Technology

2018-012

DOI:10.11484/jaea-technology-2018-012

## Preliminary Combustion Analyses using OpenFOAM

---

Thwe Thwe Aung, Atsuhiko TERADA and Ryutaro HINO

Research Division for Potential Risk Reduction in Decommissioning  
Collaborative Laboratories for Advanced Decommissioning Science  
Fukushima Research Institute  
Sector of Fukushima Research and Development

January 2019

Japan Atomic Energy Agency

日本原子力研究開発機構

JAEA-Technology

本レポートは国立研究開発法人日本原子力研究開発機構が不定期に発行する成果報告書です。  
本レポートの入手並びに著作権利用に関するお問い合わせは、下記あてにお問い合わせ下さい。  
なお、本レポートの全文は日本原子力研究開発機構ホームページ (<https://www.jaea.go.jp>)  
より発信されています。

国立研究開発法人日本原子力研究開発機構 研究連携成果展開部 研究成果管理課  
〒319-1195 茨城県那珂郡東海村大字白方2番地4  
電話 029-282-6387, Fax 029-282-5920, E-mail:ird-support@jaea.go.jp

This report is issued irregularly by Japan Atomic Energy Agency.  
Inquiries about availability and/or copyright of this report should be addressed to  
Institutional Repository Section,  
Intellectual Resources Management and R&D Collaboration Department,  
Japan Atomic Energy Agency.  
2-4 Shirakata, Tokai-mura, Naka-gun, Ibaraki-ken 319-1195 Japan  
Tel +81-29-282-6387, Fax +81-29-282-5920, E-mail:ird-support@jaea.go.jp

© Japan Atomic Energy Agency, 2019

## Preliminary Combustion Analyses using OpenFOAM

Thwe Thwe Aung, Atsuhiko TERADA and Ryutaro HINO  
Research Division for Potential Risk Reduction in Decommissioning  
Collaborative Laboratories for Advanced Decommissioning Science  
Fukushima Research Institute, Sector of Fukushima Research and Development  
Japan Atomic Energy Agency  
Oarai-machi, Higashi Ibaraki-gun, Ibaraki-ken

(Received November 19, 2018)

Besides the risks related to the Nuclear Power Plant during the production process or severe incident, the risks from nuclear wastes have also the possibility to threaten the society. Under long-term storage of nuclear wastes including low-level and high-level wastes, hydrogen may be spontaneously generated from corrosion of metal wastes and container wall itself, and from radiolysis of water in the waste. For the sake of hydrogen safety and the risk reduction of environmental contamination, we have started to investigate the behavior and characteristics of hydrogen combustion and explosion in waste vessel/container.

In this report, as the preliminary step, we performed numerical simulation for temperature, velocity and carbon dioxide distributions of methane combustion in simple container by applying open source CFD software package, OpenFOAM, as a computational tool. For combustion scenario, FireFoam solver with LES frame was used to execute this model. The container **A** has one cubic meter in volume. To clarify the distribution behaviors depending on the size of container, the height of container was increased to 1.5m (second container **B1**). The dimension of inlet on base of the container was increased from 0.2m×0.006m×0.2m to 0.4m×0.006m×0.4m in higher container (third container **B2**). The inlet velocity, initial temperature and pressure was set to 0.01m/s, 300K, 1.01325×10<sup>5</sup>Pa, respectively for all cases. The air inside of the container was composed of 23 % O<sub>2</sub> and 77% N<sub>2</sub> in weight. The computational time was set to 20s. As the results, the average temperature increased when the height of container increased and inlet size became larger. The obtained results from the simulation of diffusion behavior of methane, hydrogen and helium by the FireFoam solver showed that helium diffused faster than other two gases. By using the XiFoam solver which is compactable premixed combustion, flame propagation radius was obtained for hydrogen-air premixed flame inside of the cubic combustion chamber under stoichiometric conditions.

Keywords: Combustion, Analyses, Hydrogen, OpenFOAM, Nuclear Waste

## OpenFOAM を用いた予備燃焼解析

日本原子力研究開発機構 福島研究開発部門 福島研究開発拠点  
廃炉国際共同研究センター 廃炉リスク管理研究ディビジョン  
トエ トエ アウン、寺田 敦彦、日野 竜太郎

(2018年11月19日 受理)

原子力発電所に関連するシビアインシデントや製造工程のリスク以外に、原子力廃棄物のリスクも社会を脅かす可能性がある。低レベル及び高レベルの放射性廃棄物を含む核廃棄物の長期保管下では、金属廃棄物の腐食や容器壁自体の腐食及び廃棄物中の水の放射線分解により水素が自発的に発生する。そこで、水素安全及び環境汚染のリスク低減のために、放射性廃棄物容器における水素燃焼爆発の挙動と特性を調べることにした。

本報告書では、予備ステップとして、オープンソース CFD ソフトウェアパッケージである OpenFOAM を計算ツールとして適用し、簡易コンテナ内におけるメタン燃焼の温度、速度と二酸化炭素分布を調べる数値解析シミュレーションを行った。燃焼シナリオでは、このモデルを実行するために LES フレームを備えている FireFoam ソルバーを使用した。容器 A の容積は  $1\text{m}^3$  で設定し、容器 B1 の容積を A の 1.5 倍に増加させ、容器の大きさによる分布挙動を明らかにした。さらに、容器 B2 では、基部上のガス流入する入口の寸法を  $0.2\text{m} \times 0.006\text{m} \times 0.2\text{m}$  から  $0.4\text{m} \times 0.006\text{m} \times 0.4\text{m}$  に増加し、その影響を調べた。全てのシミュレーションにおいて、ガス流入速度、初期温度及び圧力は、それぞれ  $0.01\text{m/s}$ 、 $300\text{K}$ 、 $1.01325 \times 10^5 \text{ Pa}$  に設定した。容器内の空気は重量で 23% の  $\text{O}_2$  と 77% の  $\text{N}_2$  から構成され、計算時間は 20 秒に設定した。結果として、容器の高さ及び流入口のサイズが大きくなるとともに平均温度が上昇することが分かった。一方、FireFoam ソルバーで行ったメタン、水素及びヘリウムの拡散挙動シミュレーションによると、メタンや水素よりもヘリウムのほうが速く拡散することが明らかにした。予混合燃焼については XiFoam ソルバーを利用することにより、化学量論的条件下で立方体燃焼容器における水素空気予混合火炎の火炎伝播半径が得られた。

Contents

1. Introduction	1
2. Outline of OpenFOAM	3
2.1 Features of OpenFOAM	3
2.2 Structure of OpenFOAM	3
2.3 Setup of case file in OpenFOAM	4
2.4 Solvers for Combustion Modellings in OpenFOAM	5
2.5 Installation of OpenFOAM	6
3. Preliminary Numerical Simulations by FireFOAM Solver	7
3.1 Case Setup for Methane Combustion	7
3.2 Geometry Creation	8
3.3 Mesh Generation	9
3.4 Initial and Boundary Conditions	11
3.5 Numerical Simulation	12
3.6 Results and Discussion	14
3.7 Simulation of Gas Diffusion by FireFOAM Solver	28
4. Preliminary Numerical Simulaiton by XiFOAM Solver	35
4.1 Case Setup for Hydrogen-Air Combustion	35
4.2 Initial and Boundary Conditions	36
4.3 Numerical Simulation	36
4.4 Results and Discussion	37
5. Concluding Remarks	42
References	44
Appendix	45

目次

1. 序論	1
2. OpenFOAM の概要	3
2.1 OpenFOAM の特徴	3
2.2 OpenFOAM の構成	3
2.3 OpenFOAM でのケースファイルの設定	4
2.4 OpenFOAM における燃焼モデルソルバー	5
2.5 OpenFOAM のインストール方法	6
3. FireFOAM ソルバーを用いる予備数値シミュレーション	7
3.1 メタン燃焼のケースセットアップ	7
3.2 ジオメトリ作成	8
3.3 メッシュ生成	9
3.4 初期・境界条件	11
3.5 予備数値シミュレーション	12
3.6 シミュレーション結果と議論	14
3.7 FireFOAM ソルバーによるガス拡散のシミュレーション	28
4. XiFOAM ソルバーを用いる予備数値シミュレーション	35
4.1 水素・空気予混合燃焼のケースセットアップ	35
4.2 初期・境界条件	36
4.3 予備数値シミュレーション	36
4.4 シミュレーション結果と議論	37
5. 結言	42
参考文献	44
付録	45

List of Figures

Fig. 2.1	Overall structure of OpenFOAM .....	4
Fig. 2.2	Basic structure of a case directory .....	4
Fig. 3.1	Structure of case file for FireFOAM .....	7
Fig. 3.2	Geometries for combustion model .....	8
Fig. 3.3	Sketch of mesh generation block .....	9
Fig. 3.4	Mesh configuration of container A .....	11
Fig. 3.5	Mesh configuration of container B1 and B2 .....	11
Fig. 3.6	Distribution of temperature in container A at $t = 0.1, 0.5, 1.0, 4.0, 6.0, 8.0, 10.0,$ $12.0, 14.0, 16.0, 18.0, 20.0s.$ .....	15
Fig. 3.7	Distribution of temperature in container B1 at $t = 0.1, 0.5, 1.0, 4.0, 6.0, 8.0,$ $10.0, 12.0, 14.0, 16.0, 18.0, 20.0s.$ .....	16
Fig. 3.8	Distribution of temperature in container B2 at $t = 0.1, 0.5, 1.0, 4.0, 6.0, 8.0,$ $10.0, 12.0, 14.0, 16.0, 18.0, 20.0s.$ .....	17
Fig. 3.9	Distribution of velocity magnitude in container A at $t = 0.1, 0.5, 1.0, 4.0, 6.0,$ $8.0, 10.0, 12.0, 14.0, 16.0, 18.0, 20.0s.$ .....	18
Fig. 3.10	Distribution of velocity magnitude in container B1 at $t = 0.1, 0.5, 1.0, 4.0, 6.0,$ $8.0, 10.0, 12.0, 14.0, 16.0, 18.0, 20.0s.$ .....	19
Fig. 3.11	Distribution of velocity magnitude in container B2 at $t = 0.1, 0.5, 1.0, 4.0, 6.0,$ $8.0, 10.0, 12.0, 14.0, 16.0, 18.0, 20.0s.$ .....	20
Fig. 3.12	Distribution of carbon dioxide mass fraciton in container A at $t = 0.1, 0.5, 1.0,$ $4.0, 6.0, 8.0, 10.0, 12.0, 14.0, 16.0, 18.0, 20.0s.$ .....	21
Fig. 3.13	Distribution of carbon dioxide mass fraciton in container B1 at $t = 0.1, 0.5, 1.0,$ $4.0, 6.0, 8.0, 10.0, 12.0, 14.0, 16.0, 18.0, 20.0s.$ .....	23
Fig. 3.14	Distribution of carbon dioxide mass fraciton in container B2 at $t = 0.1, 0.5, 1.0,$ $4.0, 6.0, 8.0, 10.0, 12.0, 14.0, 16.0, 18.0, 20.0s.$ .....	25
Fig. 3.15	Time history of the maximum values of (a) temperature $T[K]$ , velocity magnitude $U [m/s]$ , and (c) $CO_2$ mass fraction at each output time step (0.1, 0.2, ... , 20) .....	27
Fig. 3.16	Diffusion behavior of methane into air at $t= 0.5, 1.0, 1.5, 2.0, 2.5, 3.0, 3.5, 4.0,$ $4.5, 5.0, 5.5, 6.0, 6.5, 7.0, 7.5, 8.0, 8.5, 9.0, 9.5, 10.0s$ .....	28
Fig. 3.17	Diffusion behavior of hydrogen into air at $t= 0.5, 1.0, 1.5, 2.0, 2.5, 3.0, 3.5, 4.0,$ $4.5, 5.0, 5.5, 6.0, 6.5, 7.0, 7.5, 8.0, 8.5, 9.0, 9.5, 10.0s$ .....	30
Fig. 3.18	Diffusion behavior of helium into air at $t= 0.5, 1.0, 1.5, 2.0, 2.5, 3.0, 3.5, 4.0,$ $4.5, 5.0, 5.5, 6.0, 6.5, 7.0, 7.5, 8.0, 8.5, 9.0, 9.5, 10.0s$ .....	32
Fig. 3.19	Comparison of the diffusion of methane, hydrogen an helium into air by FireFoam solver .....	34

Fig. 4.1	Mesh configuration of the one-eighth of combustion vessel .....	35
Fig. 4.2	Temperature distribution of H <sub>2</sub> -air premixed flame ( $\phi=1.0$ ) at 0.001, 0.002, 0.004, 0.006, 0.008, 0.01s .....	38
Fig. 4.3	Distribution of turbulent flame speed of H <sub>2</sub> -air premixed flame ( $\phi=1.0$ ) at 0.001, 0.002, 0.004, 0.006, 0.008, 0.01s .....	39
Fig. 4.4	Distribution of laminar flame speed of H <sub>2</sub> -air premixed flame ( $\phi=1.0$ ) at 0.001, 0.002, 0.004, 0.006, 0.008, 0.01s .....	40
Fig. 4.5	Burned-gas temperature and pressure of H <sub>2</sub> -air premixed flames ( $\phi=1.0$ ) .....	41
Fig. 4.6	Flame wrinkling factor, turbulent flame speed and laminar flame of H <sub>2</sub> -air premixed flame ( $\phi=1.0$ ) .....	41
Fig. 4.7	Flame propagation radius of H <sub>2</sub> -air premixed flame ( $\phi=1.0$ ) .....	41

## 1. Introduction

In the field of Nuclear Reactor Safety (NRS), researches on distribution and combustion of hydrogen become more active recently because of the threat on accumulation of large quantities of hydrogen in the containment of water cool reactors during severe accidents. Overheating of the core cladding during the accident lets the high temperature Zircaloy cladding to react with steam and produce hydrogen. Hydrogen may also be generated from the molten corium-concrete interaction (MCCI) in which zirconium reacts with water and produces hydrogen, or from reactor core degradation, and released to the reactor coolant system, eventually the containment, and mixes with air and becomes the combustible mixture. Depending on the concentration of hydrogen and nature of ignition sources, geometry, pressure, temperature and other factors, accelerated flames, deflagration or even detonations can occur and those lead to damage reactor safety systems and integrity of containment wall. Thus, the risk of hydrogen combustion in the containment is one of the major threats in NRS. Hydrogen explosion during the severer accidents of Fukushima Nuclear Power Plant made more attentions on hydrogen risk in NPP [1].

Besides the risks related to the NPP during the production process, risks from nuclear wastes also threaten the society [2]. Under long-term storage of nuclear wastes including low-level and high-level wastes, hydrogen may be spontaneously generated from corrosion of metal wastes and container wall itself, and from radiolysis of water in the waste [3]. It is important to be aware of the risk of hydrogen combustion and explosion during storage, handling and shipping of waste containers. Hydrogen generation rate in various waste vessels was studied in order to confirm the limit of hydrogen concentration [4][5][6]. Furthermore, generation of methane-rich gas together with hydrogen and carbon dioxide from the degradation of organics and anaerobic metal corrosion in low- and intermediate-level nuclear waste (LILW) is also important in nuclear waste repositories [7]. However, the data on the study ahead of hydrogen generation and accumulation stages i.e. combustion and explosion of hydrogen, is rare to find.

For the sake of hydrogen safety and the risk reduction of environmental contamination, we aim to investigate the behavior and characteristics of hydrogen combustion and explosion in waste vessel/container. Numerical simulation is chosen on this purpose, since simulation can assist to experiments and it is also important as a complementary work in combustion and explosion research. To perform numerical simulation, OpenFOAM which is an open source CFD software developed by OpenCFD Limited will be applied [8]. In this report, we perform the numerical simulation of methane combustion in container and investigate temperature, velocity and carbon dioxide fraction as the preliminary numerical simulation.

To use OpenFOAM solvers as the application tools for preliminary step of numerical

simulation for hydrogen combustion in the vessel, we need to understand and to be familiar with the insides of OpenFOAM, that is, usage of utilities and solvers within the short period of time with the less use of third party applications. For this, test running with supported tutorials is the most reliable way for the beginner user of OpenFOAM. Running the various types of original tutorials for different solvers will let us grow our knowledge at the very first stage. And then, the relevant solvers should be able to choose for our own specific models on the research objectives. Thus, we performed the numerical simulations of methane combustion by FireFoam solver prior to continue the hydrogen combustion in the first case. One more reason for choosing methane is that which is also a gas generated and released in nuclear waste vessel [7]. Next, diffusions of methane, hydrogen and helium into air were simulated by FireFoam solver. As the second case, numerical simulation of the combustion of premixed hydrogen-air in the cubic combustion chamber based on the case in which released hydrogen gas is mixed with exiting air in the waste vessel was performed by XiFoam solver.

## 2. Outline of OpenFOAM

### 2.1 Features of OpenFOAM

OpenFOAM which stands for Open Source Field Operation And Manipulation, is an open source numerical simulation with extensive CFD developed by OpenCFD Ltd since 2004 [8]. The new version of OpenFOAM is released every six months in June and December. OpenFOAM is a free software under the GNU General Public License. Since the OpenFOAM is an open source application tool, it is downloadable from official web site of OpenCFD Limited. Without any cost, users can redistribute, extensively modify and customize the models/codes of OpenFOAM under the terms of License. According to the Ref.[8], *“OpenFOAM has an extensive range of features to simulate anything from turbulent flows in automotive aerodynamics, to fires and fire suppression in buildings, involving combustion, chemical reactions, heat transfer, liquid sprays and films. It includes tools for meshing in and around complex geometries, and for data processing and visualization, and more. Almost all computations can be executed in parallel as standard to take full advantage of today’s multi-core processors and multi-processor computers.”*

Since Geometry creation module is not included in OpenFOAM, the user can use other application tools or packages for geometry creation and created geometry can be imported to OpenFOAM. Mesh conversion utilities in OpenFOAM can convert the format of generated mesh with other packages to OpenFOAM format. Syntax for tensor operations and partial differential equations which close to the governing equations that we want to be solved, is included in the features of OpenFOAM.

### 2.2 Structure of OpenFOAM

OpenFOAM is a C++ library and it has two applications: solvers and utilities. User can choose the relevant solver to solve specific problem. Relating to the data manipulation, the tasks are performed by using utilities. The operation of OpenFOAM includes case setup, wide range of available functions, running applications and postprocessing the results. The overall structure of OpenFOAM is as shown in Fig.2.1.

In preprocessing, to generate mesh, we can use either the mesh generators supplied with OpenFOAM or mesh conversion tools for mesh data that generated by other applications such as Fluent, STAR-CD, ANSYS, GAMBIT and CFX. In postprocessing, we can use ParaView, an open source visualization application [9], which can be called by postprocessing utility paraFoam in OpenFOAM. There are also other applications such as EnSight, FieldView and Fluent for postprocessing.

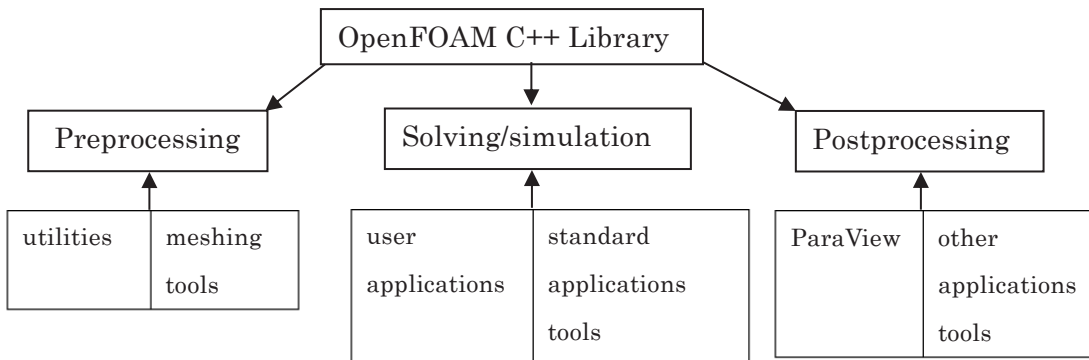


Fig.2.1 Overall structure of OpenFOAM [8].

### 2.3 Setup of case file in OpenFOAM

For running application, a case file which contains minimum set of required files needs to be created. A case file has basically three directories: time directories which contain individual files of data such as initial and boundary conditions for particular fields of specific problem; constant directory which contains subdirectory *polyMesh* for meshing and specific files for physical properties of the field for simulation; system directory which contains *controlDict* file to set parameters for run time, data input and output, *fvSchemes* for discretization schemes, and *fvSolution* for equation solvers [8]. Figure 2.2 shows the basic structure of a case directory.

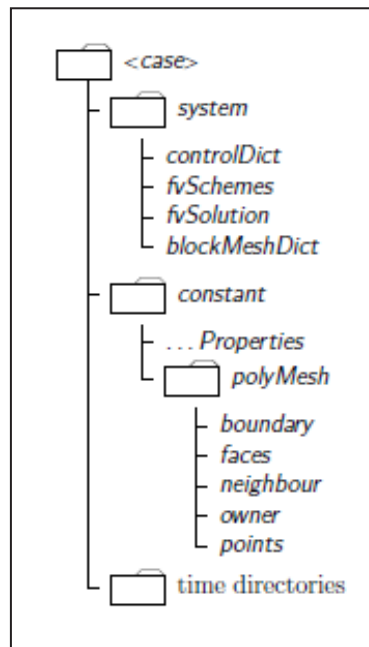


Fig.2.2 Basic structure of a case directory [8].

## 2.4 Solvers for Combustion Modellings in OpenFOAM

In OpenFOAM, choosing the most relevant solver is important to obtain the correct results for specific model being solved. The standard solvers in OpenFOAM are available for compressible flow, incompressible flow, multiphase flow, combustion, heat transfer and buoyancy-driven flows, and particle-tracking flows. To perform the numerical simulations for combustion modellings, solvers can be chosen depending on whether the modelling is for premixed, partially-premixed or non-premixed regimes. The list of standard solvers for combustion modellings are described in Table 2.1.

Table 2.1 Standard solvers for combustion modellings [8].

chemFoam	Solver for chemistry problems, designed for use on single cell cases to provide comparison against other chemistry solvers, that uses a single cell mesh, and fields created from the initial conditions
coldEngineFoam	Solver for cold-flow in internal combustion engines
engineFoam	Solver for internal combustion engines
fireFoam	Transient solvers for fires and turbulent diffusion flames with reacting particle clouds, surface film and pyrolysis modelling
PDRFoam	Solver for compressible premixed/partially-premixed combustion with turbulence modelling
reactingFoam	Solver for combustion with chemical reactions
rhoReactingBuoyantFoam	Solver for combustion with chemical reaction using density based thermodynamic package with enhanced buoyancy treatment
rhoReactingFoam	Solver for combustion with chemical reactions using density based thermodynamics package
XiFoam	Solver for compressible premixed/partially-premixed combustion with turbulence modelling
XiDyMFoam	Solver for compressible premixed/partially-premixed combustion with turbulence modelling

Since default XiFoam and XiDyMFoam are intended for compressible premixed/partially-premixed modellings, and fireFoam and reactingFoam which includes rhoReactingFoam and rhoReactingBuoyantFoam are available for non-premixed modellings. Although ReactingFoam solvers are implemented for detail chemical reactions, radiation transport equation is not equipped in default solvers for combustion flow simulations. However,

users can add required equations to existing codes for solving their intended problem modellings. Default fireFoam solver can calculate radiative characteristics. There are two version of fireFoam code: (1) solver for transient fire and diffusion flame simulation (Open CFD official release); (2) solver modified and maintained by FM Global for fire research [10].

Besides the standard combustion solvers, ddtFoam solver which is developed to simulate the deflagration-to-detonation transition, is also available to download directly from Ref.[13].

## 2.5 Installation of OpenFOAM

OpenFOAM is available to download from official web sites of openfoam.org and openfoam.com by user's choice on Linux, Mac or Windows versions. The latest version of OpenFOAM-v1806 was released on 29<sup>th</sup> June 2018. Every new version includes improvements of codes, new-tools, -utilites, and -modellings. The detailed instructions are described at the web page of OpenFOAM, so that user can easily install the downloaded file following the instructions on their machine, and can start with supported tutorials. However, some solvers, e.g. ddtFoam does not match with newly versions of OpenFOAM because it was developed to use in older version of 2.1.1 [13]. Thus, older versions are still useful in some specific modellings and simulations. For our preliminary numerical simulation, OpenFOAM-v1712 for Window version was downloaded from openfoam.com [8] and installed on Dell Precision Tower 5810, with RAM 64.0GB, Inel Xeon CPU E5-1620 v4@ 3.5GHz.

### 3. Preliminary Numerical Simulations by FireFOAM Solver

#### 3.1 Case Setup for Methane Combustion

In this numerical calculation, we considered the methane combustion model in which fuel gas was sinking or entering from the base of the vessel/container through the inlet hole. The air was assumed being inside of the container. Thus, flame type was not a premixed type but a diffusion one. Although many types of standard combustion solvers are possible to choose, we chose default fireFoam solver which supported methane combustion, to solve this diffusion combustion model based on compressible flow. Default FireFOAM uses the reaction type of irreversible infinite model for one step combustion reaction, and detail chemical reaction is excluded. Thus, the running or compilation time for simple model is less compared with that for the model of detail chemical reaction. Moreover, radiative characteristics can be calculated without changing or modifying any codes in default FireFOAM.

Boundary conditions and initial fields for pressure  $p$ , temperature  $t$ , velocity  $U$ , turbulent coefficient  $k$  and constant of incident radiation field  $G$  are included in time directory. Each field is always initialized and the output is stored in 0 directory (t=0s), and the other time directories are used to store the simulation results at each output time. The constant directory and system directory contain common utilities files for fireFoam solver. The structure of the case file for FireFOAM is shown in Fig.3.1.

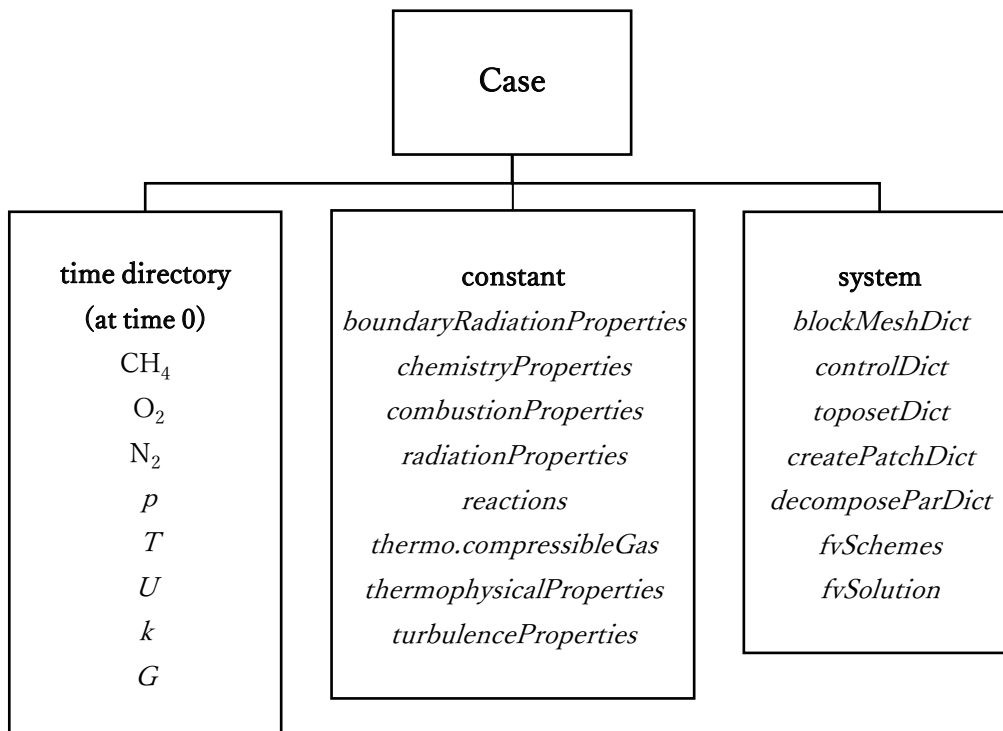


Fig.3.1 Structure of case file for FireFOAM.

*BlockMeshDict* is for generating simple meshes of blocks of hexahedral cells. *ControlDict* dictionary is for setting input parameters essential for the creation of the database and the entries represents the time control. *TopoSetDict* is operating on cellSets/faceSets/pointSets through a dictionary, for example, connecting a box to host face by *boxToFace* utility. To create patches out of selected boundary faces, *createPatchDict* utility is used. By *decomposePar* utility, mesh and fields of a case are automatically decomposed for parallel execution of OpenFOAM. Discretisation schemes used in the solution are set in *fvSchemes*, i.e. setting numerical schemes for terms that appeared in applications. *FvSolution* which contains a set of subdictionaries controls the equation solvers, tolerances and algorithms.

### 3.2 Geometry Creation

In preprocessing, creation of geometry model and mesh generation were performed. 3-dimensional geometry was setup and the geometries are shown in Fig.3.2.

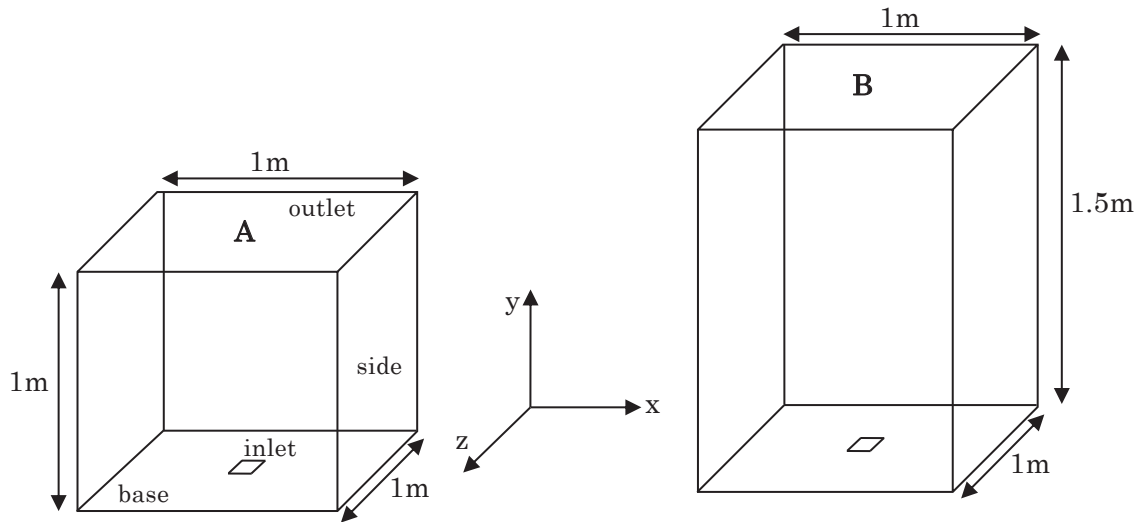


Fig.3.2 Geometries for combustion model.

The size of rectangular shape container **A** is  $1.0\text{m} \times 1.0\text{m} \times 1.0\text{m}$  and that of **B** (**B1** and **B2**) is  $1.0\text{m} \times 1.5\text{m} \times 1.0\text{m}$  in length  $\times$  height  $\times$  width (x, y, z in direction). There are 6 faces and 12 edges on each container. For the fuel inlet,  $0.2\text{m} \times 0.006\text{m} \times 0.2\text{m}$  bounding box is set on the center of base of **A** and **B1**. The size of inlet is increased to  $0.4\text{m} \times 0.006\text{m} \times 0.4\text{m}$  in **B2**.

### 3.3 Mesh Generation

All geometries were generated in 3-dimensional Cartesian coordinate system. A uniform mesh of 60 cells was used on one cubic meter face, thus 90 cells for y-z face in **B1** and **B2** container. Sketch of mesh generation block for **A** is shown in Fig.3.3. The configuration of mesh generation for **A** is shown in Fig.3.4, and for **B1** and **B2** are in Fig.3.5.

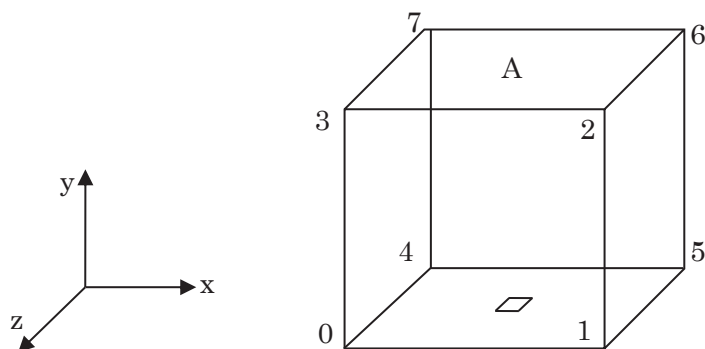


Fig.3.3 Sketch of mesh generation block.

The simple mesh generator, *blockMesh* generated the mesh. Block defining, vertices coordinates, and scale conversion were specified in block mesh dictionary file. The contents inside of the *blockMeshDict* of container **A** is as follows:

```

convertToMeters 1; // m used in the file
vertices
(
  (-0.5 0 -0.5) //vertice 0
  (0.5 0 -0.5) //vertice 1
  (0.5 1 -0.5) //vertice 2
  (-0.5 1 -0.5) //vertice 3
  (-0.5 0 0.5) //vertice 4
  (0.5 0 0.5) //vretice 5
  (0.5 1 0.5) //vertice 6
  (-0.5 1 0.5) //verice 7
);
blocks
(
  hex (0 1 2 3 4 5 6 7) (60 60 60) simpleGrading (1 1 1)
); //60, 60, 60 grid points in x, y, z axis respectively
edges
(

```

```

);
boundary
(
  base
  {
    type patch;
    faces
    (
      (0 1 5 4)
    );
  }
  outlet
  {
    type patch;
    faces
    (
      (3 2 6 7)
    );
  }
  sides
  {
    type patch;
    faces
    (
      (0 4 7 3)
      (0 1 2 3)
      (1 5 6 2)
      (4 5 6 7)
    );
  }
);
mergePatchPairs
(
);

```

Each block was divided by *simpleGrading*(1 1 1) to get the uniform mesh. The number of grid points in each direction was set as 60, 60, 60 grid points in x, y, z direction respectively for **A** and 60, 90, 60 for **B1** and **B2**. Generated total number of cells, *nCells* on

container **A** was 216000, and that on **B1** and **B2** was 324000.

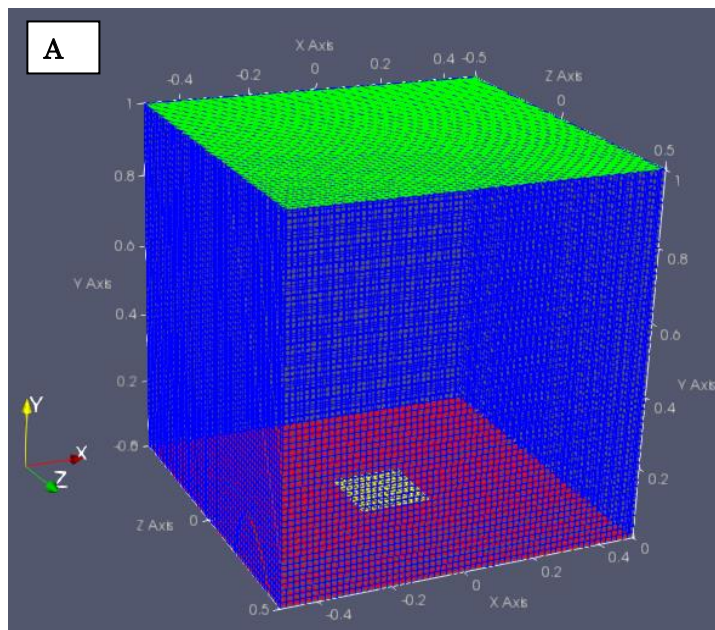


Fig.3.4 Mesh configuration of container A.

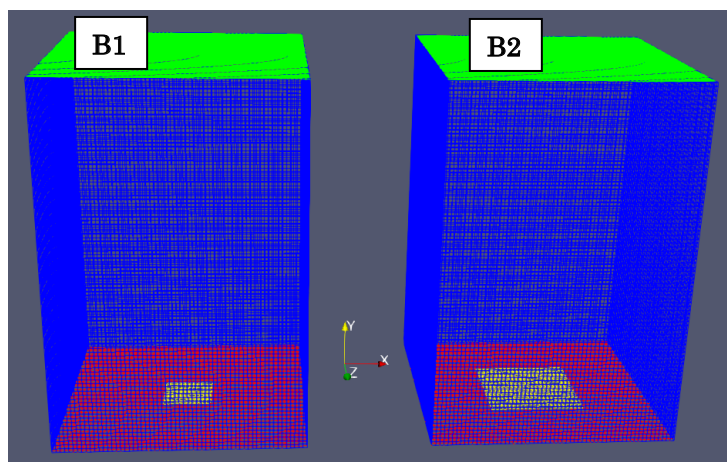


Fig.3.5 Mesh configuration of container B1 and container B2.

### 3.4 Initial and Boundary Conditions

Initial and boundary conditions were set for wall and patches i.e. inlet, base, outlet, and sides. The boundary conditions included methane ( $\text{CH}_4$ ), air (23%  $\text{O}_2$ : 77%  $\text{N}_2$ ), pressure  $p$ , temperature  $T$ , velocity  $U$  and turbulence coefficient  $k$ .  $\text{N}_2$  served as inert in the reaction. Gravitational force was considered along the y-direction. Since the case was setup to start  $t = 0\text{s}$ , the initial field data was stored in a 0 sub-directory. The inlet velocity of  $\text{CH}_4$  along the y-direction was set to  $0.01\text{ms}^{-1}$ . Initial  $T$ ,  $p$ ,  $k$  were set to 300K,  $1.01325 \times 10^5$  Pa and

1.0e-4m<sup>2</sup>/s<sup>2</sup> respectively. The pressure of sides/outlet was assigned via field assignment as *calculated*. The boundary condition *zeroGradient* applies a zero-gradient condition from the patch internal field onto the patch faces. *PressureInletOutletVelocity* means that which is applied to pressure boundaries where the pressure is specified. *NoSlip* for velocity fixes the velocity to zero at the base. *InletOut* boundary condition provides generic outflow condition, with specified inflow for the case to return flow [11]. Type of boundary conditions are listed in Table 3.1.

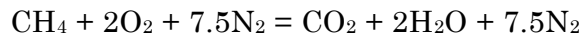
Table 3.1 Boundary conditions.

	Sides/Outlet	Inlet	Base
CH <sub>4</sub>	<i>inletOutlet</i>	1	<i>zeroGradient</i>
O <sub>2</sub>	<i>inletOutlet</i>	0	<i>zeroGradient</i>
<i>p</i>	<i>calculated</i>	1.01325×10 <sup>5</sup> Pa	<i>calculated</i>
<i>T</i>	<i>inletOutlet</i>	300K	<i>zeroGradient</i>
<i>U</i>	<i>pressureInletOutletVelocity</i>	0.01m/s	<i>noSlip</i>
<i>k</i>	<i>inletOutlet</i>	1.0e-4m <sup>2</sup> /s <sup>2</sup>	<i>zeroGradient</i>

### 3.5 Numerical simulation

The combustion model was solved by FireFOAM of OpenFOAM version, v1712 for windows 7 downloaded via openfoam.com. The solver was run in parallel on four processors of Intel Xeon CPU E5-1620 v4@ 3.5GHz, Dell Precision Tower 5810, with RAM 64.0GB.

The governing equation used in FireFAOM was Favre-average reactive Navier-Stokes equations [10][12]. The combustion model for methane in FireFOAM uses the following combustion equation with the default reaction model of *irreversibleInfiniteReaction*, in which only one reaction for equilibrium equation was taken into account. Thus, the number of iterations decreased for only five species [12].



Equation of state was *perfectGas*:  $p = \rho RT$ , which meant that ideal gas equation of state was satisfied in this case.

Thermo-physical properties for species were imported via thermo data from *thermo.compressibleGas* file which contained two sets of specific heat coefficient for high- and low-temperature range for each species taken from JANAF tables of thermodynamics. The thermodynamic model used in FireFoam was *janaf* and the relation between specific heat and temperature is as follow:

$$C_p = R(((a_4 T + a_3) * T + a_2) * T + a_1) * T + a_0)$$

where  $R$  is gas constant,  $a_0, a_1, a_2, a_3, a_4$  are specific heat coefficients. Transport model type was *sutherland* in which dynamic viscosity  $\mu$  was calculated by

$$\mu = \frac{A_s \sqrt{T}}{1 + T_s/T}$$

where  $A_s$  is a Sutherland coefficient and  $T_s$  is a Sutherland temperature which were described in *thermo.compressibleGas* file. In order to account for energy change due to reaction, the *sensibleEnthalpy* keyword was used for sensible form of energy.

The turbulence model, LES (large eddy simulation) simulation type with one equation eddy-viscosity model (kEqn) was applied and the coefficient for kEqn,  $ck$  was 0.07. The finite volume Discrete Ordinate Model (fvDOM) was used to solve radiation heat transfer equation. The coefficients of fvDOM, azimuthal angles in  $\pi/2$  on x-y (from y to x), nPhi, and polar angles in  $\pi$  (from z to x-y plane), nTheta, were set to 2. Convergence criteria for radiation iteration and maximum number of iterations were set to 0.1 and 1 respectively. The gray mean absorption emission model was used to evaluate the coefficients of absorption and emission.

There are four methods to decompose the mesh and initial field data by *decomposePar* utility in OpenFOAM. In this simulation, hierarchical method was chosen. The computational time was set to 20s for all cases. Time step interval was set to 0.0001 to achieve the maximum Courant number of 0.6. Data output time interval was set to 0.1 on run time. The detail of time control data set in *controDict* is described in Appendix. The result obtained from numerical simulation was visualized by ParaView application version 5.5, by paraFoam supported with OpenFOAM.

The commands for execution of case are as follow:

```

$<case directory>
$blockMesh
$checkMesh
$topoSet
$createPatch -overwrite
$cp -O/ph_rgh.orig O/ph_rgh
$decomposePar -force
$mpirun -np 4 fireFoam -parallel
$reconstructPar
$paraFoam //visualization and data processing
$foamToVTK //postprocessing data converter
    
```

### 3.6 Results and Discussion

We performed the numerical simulations for three types of container to study the temperature, velocity and carbon dioxide of methane combustion by using FireFoam solver of OpenFOAM. Temperature near the inlet region of the container was higher than the region away from it in the y-direction because the concentration of fuel is high near the inlet. The distribution of temperature in **B2** was most vigorous compared with that in **A** and **B1**, and **B2** had the highest average temperature. The average temperature of container **A**, **B1**, **B2** was 1724.795K, 1727.822K and 1754.117K, respectively. This means the behavior of the flame in **B2** is stronger than that in **A** and **B1**. Distribution of temperature in **A**, **B1** and **B2** are shown in Figs.3.6, 3.7 and 3.8, respectively.

To study the effects of fuel inlet size on the behavior of combustion, we performed the simulation for larger inlet size of fuel. Except early time steps, flame height in **B2** was higher than that in **B1** since velocity of the flame in former container became larger than the latter one. This is because that size of inlet in **B2** is larger than **B1**, and the increasing amount of methane entering to the container **B2** although the initial inlet velocity was set to the same value. The average velocity magnitude increased from 6.953 at **A** to 7.047 at **B1** and 8.6371 at **B2**.

As the more fuel burnt, more carbon dioxide released. Carbon dioxide fraction at **B2** was higher than that of **B1** and **A**. Figures 3.9, 3.10 and 3.11 show the distribution of velocity magnitude in **A**, **B1** and **B2**. Distribution of carbon dioxide in 3-dimensional view is shown in Fig.3.12 for **A** container, Fig.3.13 for **B1** container and Fig.3.14 for **B2** container. Figures 3.9 to 3.11 were created by using *slice* filter in ParaView normal to z-direction of the computational domain. By using *isoVolume* filter and volume rendering, Figs.3.12, 3.13 and 3.14 were obtained.

The average data values were obtained by averaging the maximum values of temperature, velocity magnitude and carbon dioxide fraction in the y-direction through the center of container at each output time interval, i.e. 0, 0.1, 0.2, ..., 20. Time history of the maximum values of temperature  $T$ , velocity magnitude  $U$ , and carbon dioxide distribution in **A**, **B1** and **B2** are shown in Fig.3.15 (a), (b) and (c), respectively.

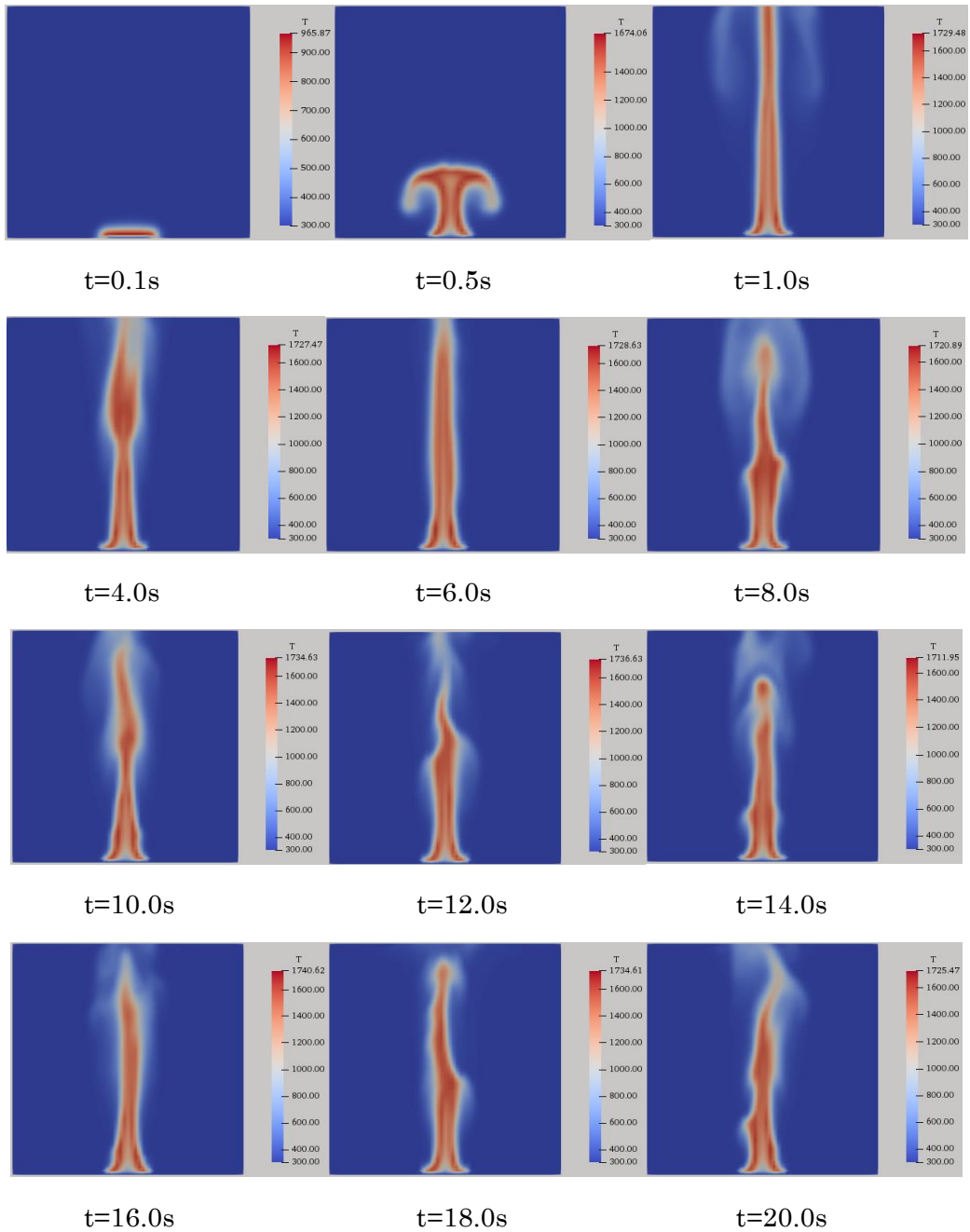


Fig.3.6 Distribution of temperature in container A at t= 0.1, 0.5, 1.0, 4.0, 6.0, 8.0, 10.0, 12.0, 14.0, 16.0, 18.0, 20.0s.

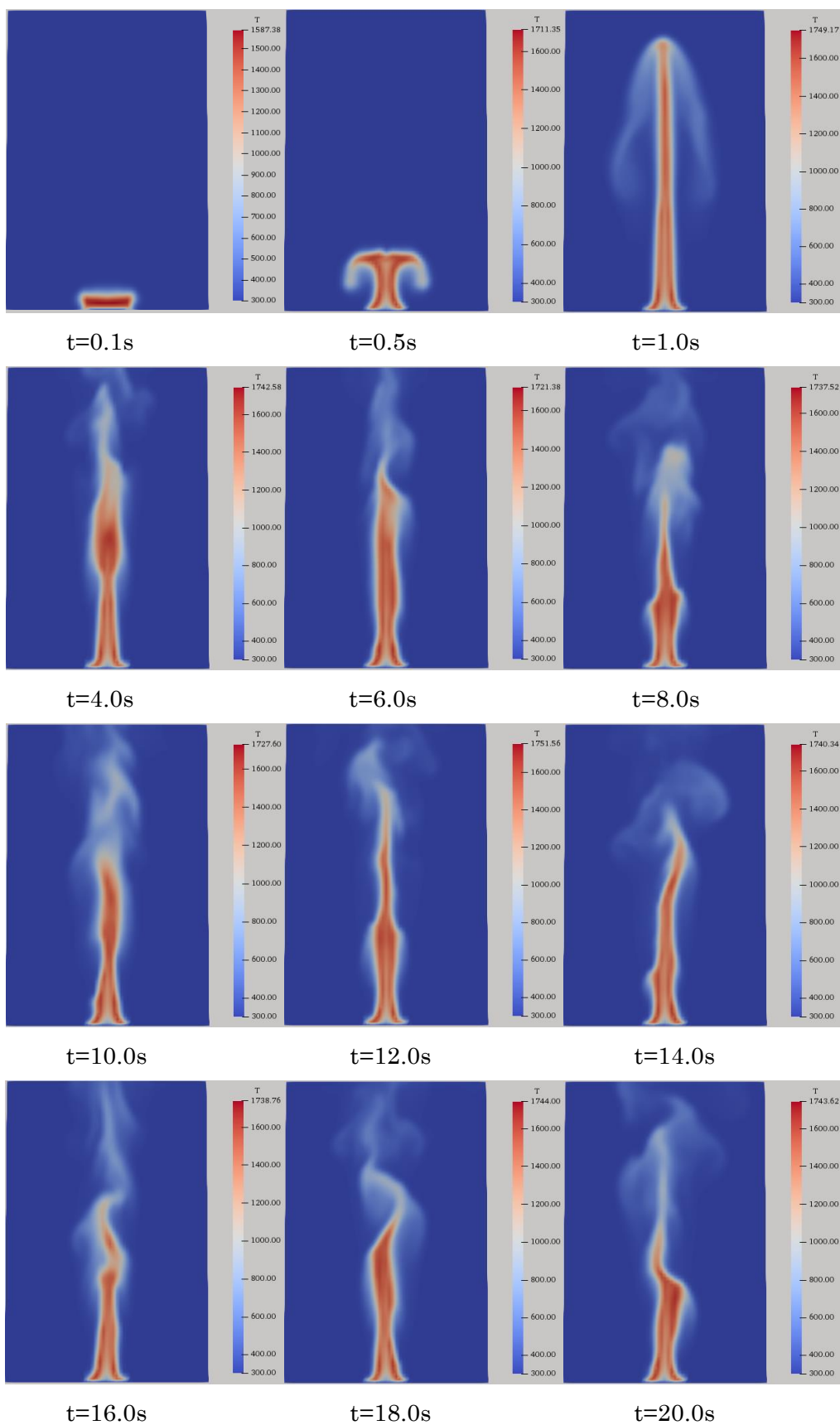


Fig.3.7 Distribution of temperature in container B1 at  $t= 0.1, 0.5, 1.0, 4.0, 6.0, 8.0, 10.0, 12.0, 14.0, 16.0, 18.0, 20.0s$ .

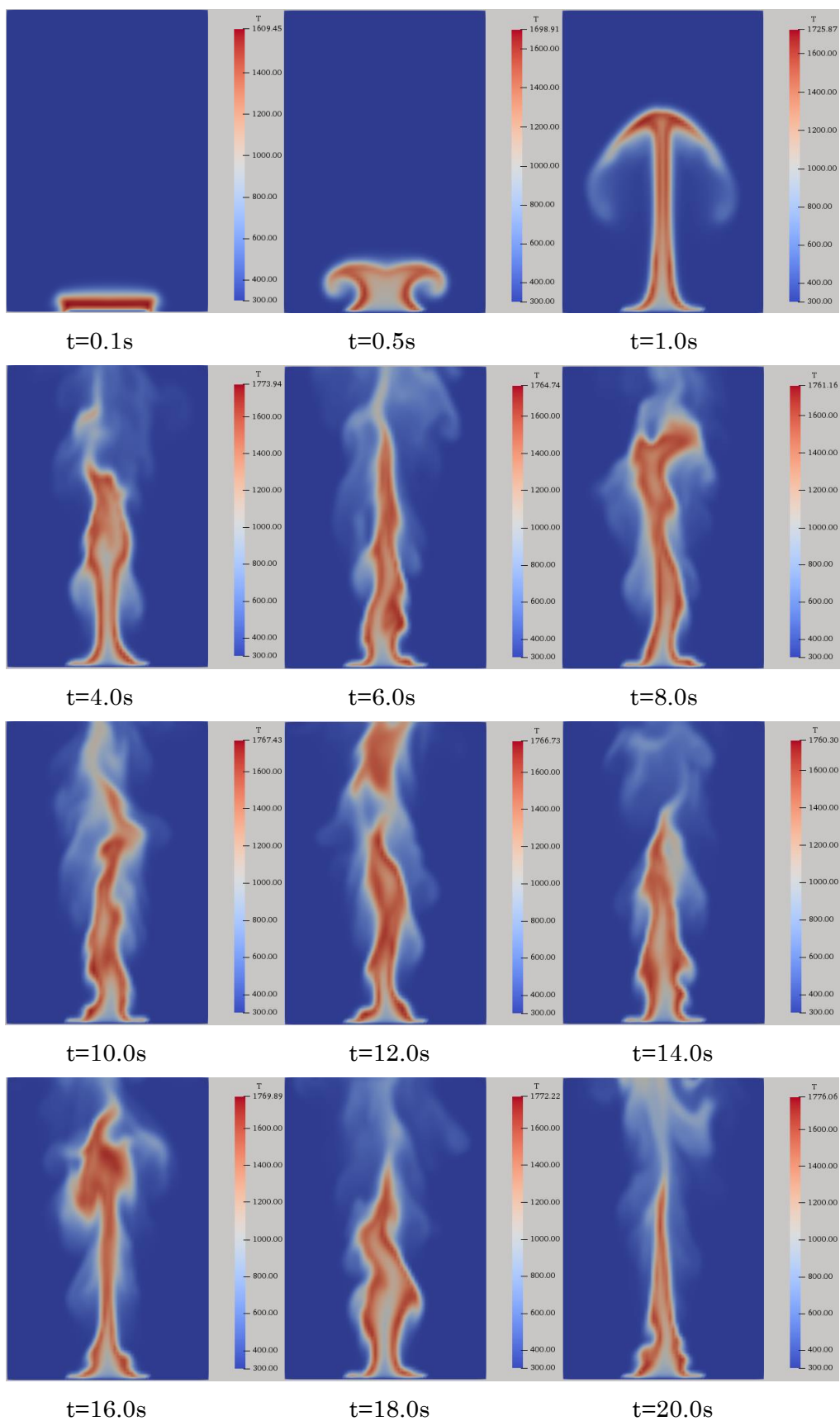


Fig.3.8 Distribution of temperature in container B2 at  $t= 0.1, 0.5, 1.0, 4.0, 6.0, 8.0, 10.0, 12.0, 14.0, 16.0, 18.0, 20.0s$ .

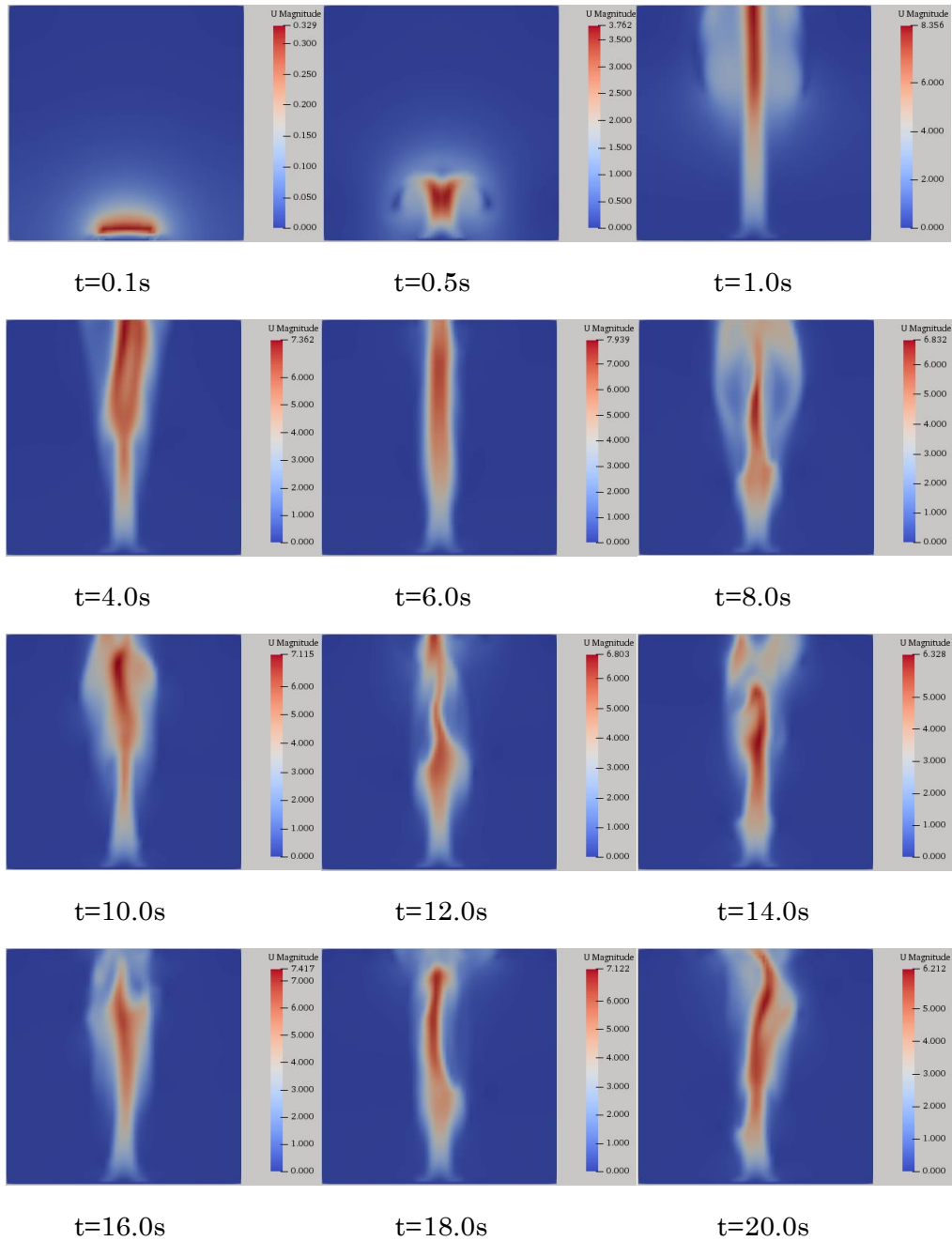


Fig.3.9 Distribution of velocity magnitude in container A at  $t= 0.1, 0.5, 1.0, 4.0, 6.0, 8.0, 10.0, 12.0, 14.0, 16.0, 18.0, 20.0s$ .

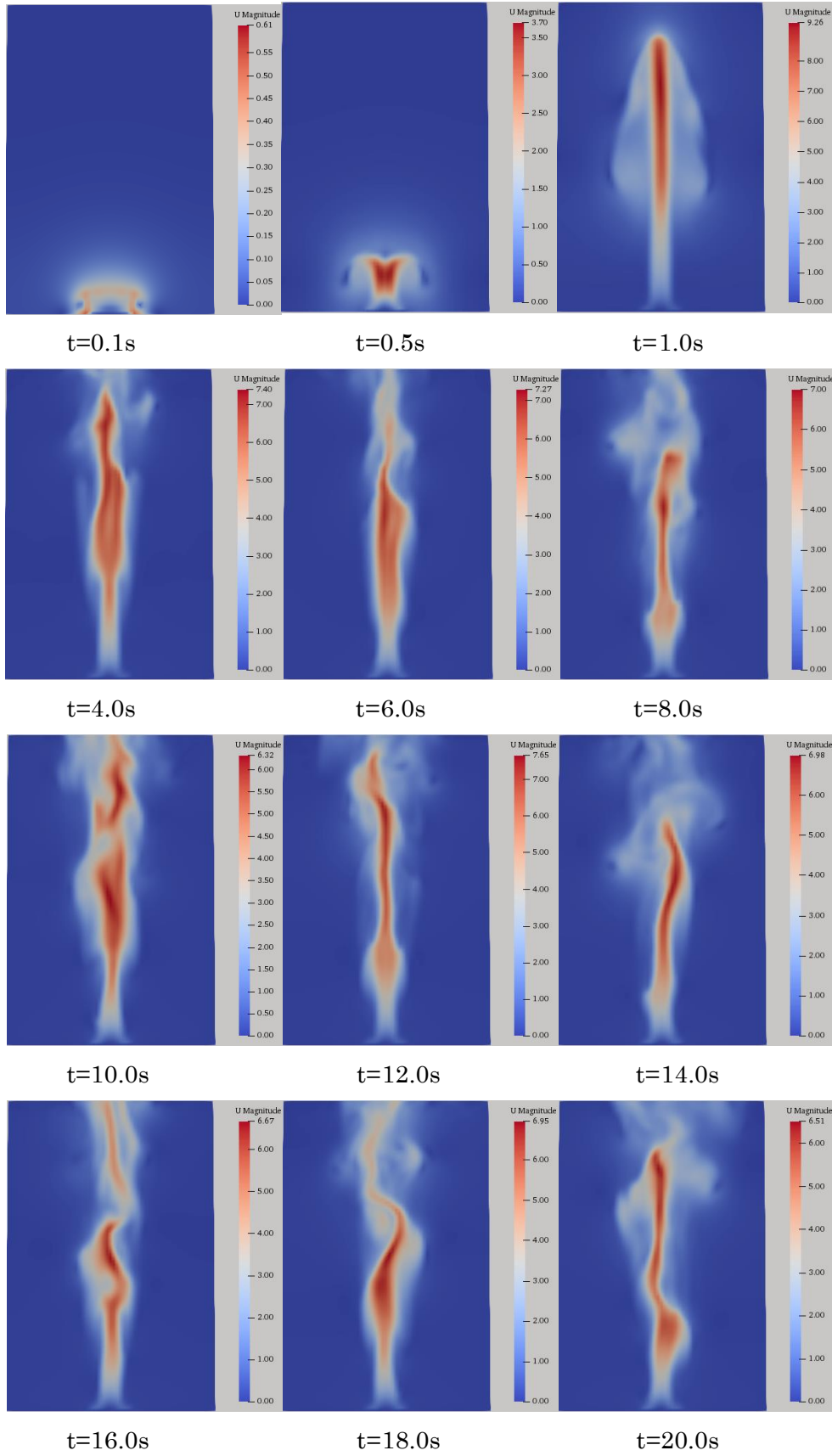


Fig.3.10 Distribution of velocity magnitude in container B1 at  $t= 0.1, 0.5, 1.0, 4.0, 6.0, 8.0, 10.0, 12.0, 14.0, 16.0, 18.0, 20.0s$ .

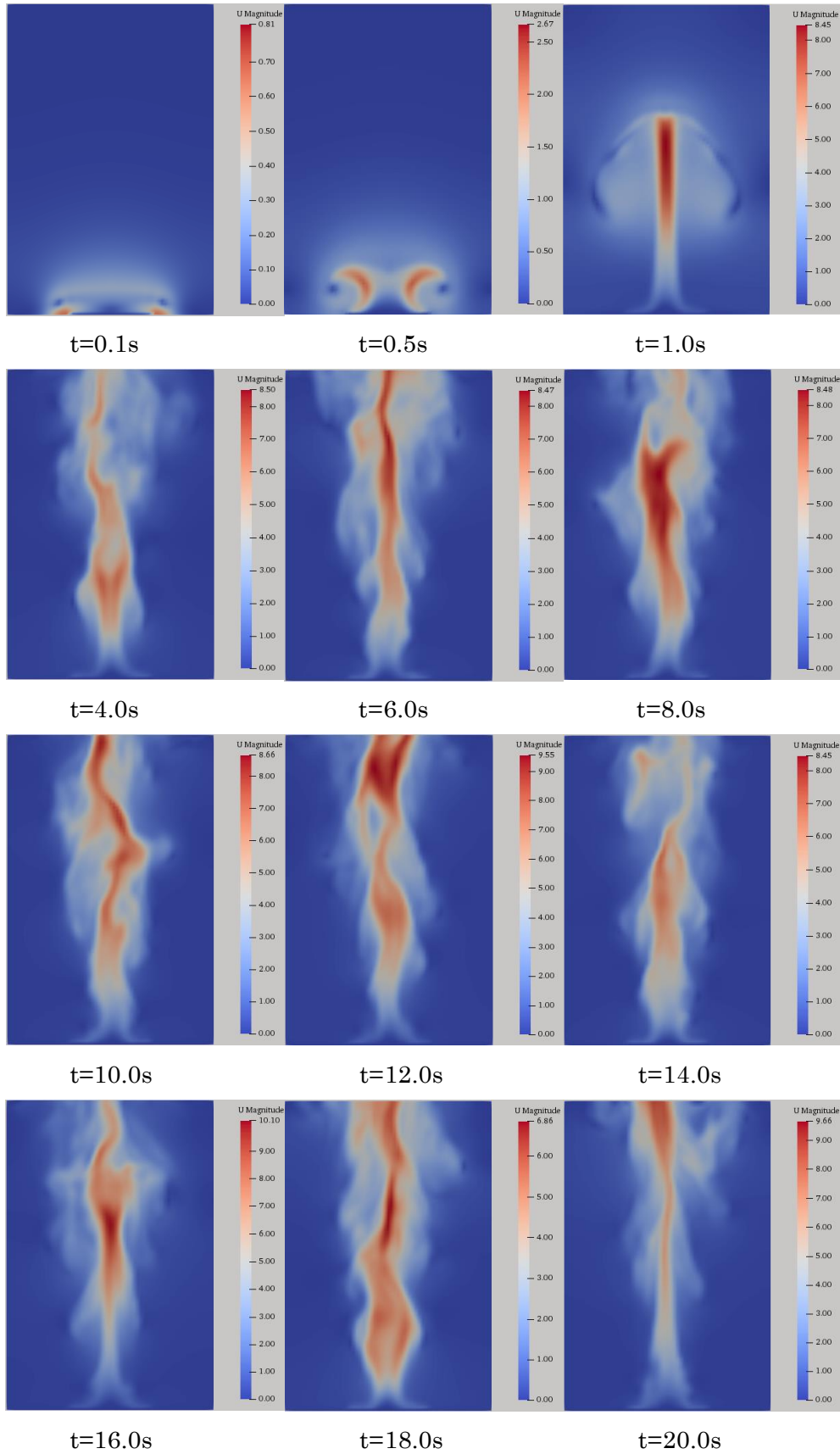


Fig.3.11 Distribution of velocity magnitude in container B2 at  $t= 0.1, 0.5, 1.0, 4.0, 6.0, 8.0, 10.0, 12.0, 14.0, 16.0, 18.0, 20.0s$ .

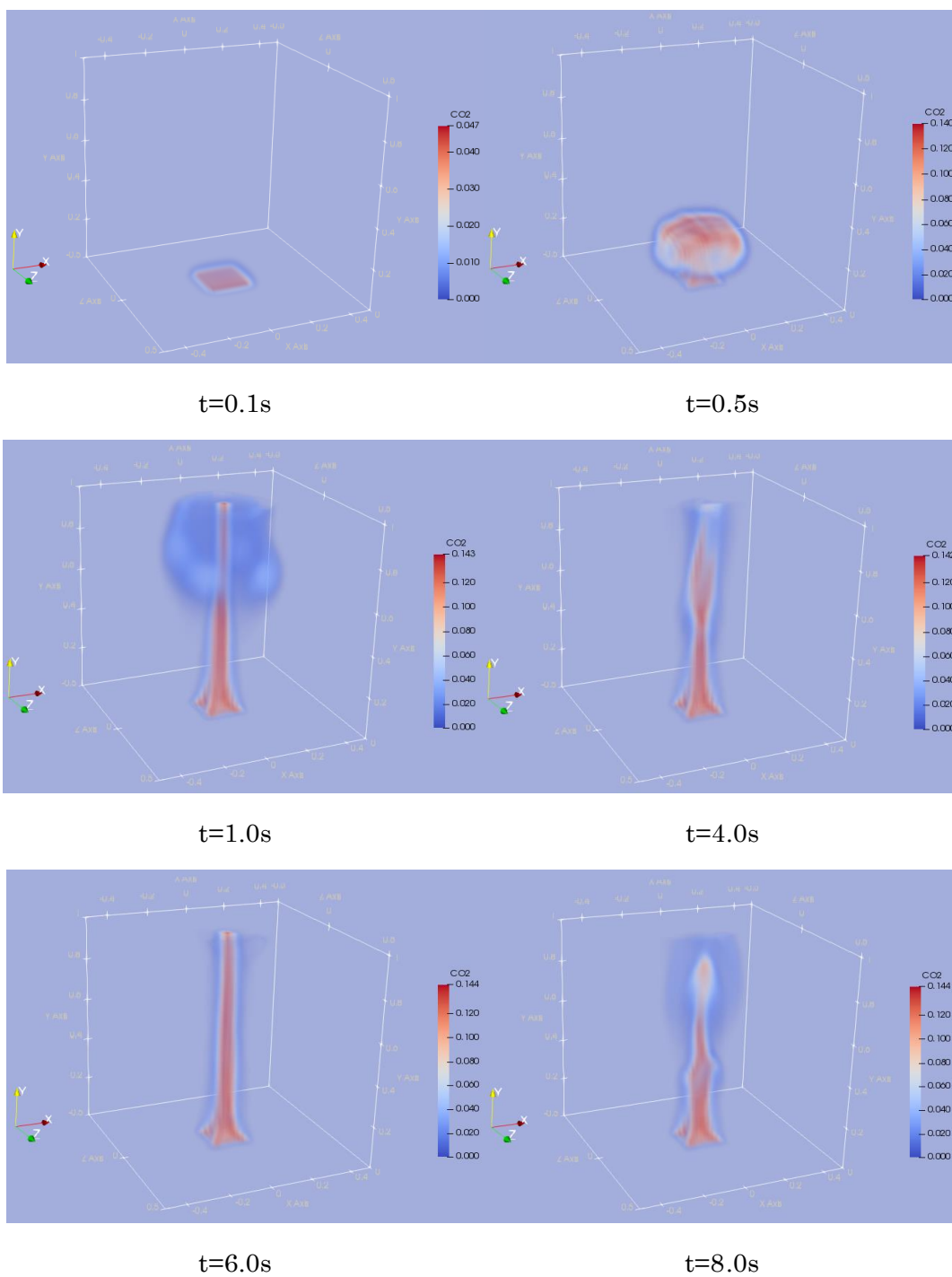


Fig.3.12 Distribution of carbon dioxide mass fraction in container A at t= 0.1, 0.5, 1.0, 4.0, 6.0, 8.0, 10.0, 12.0, 14.0, 16.0, 18.0, 20.0s (1/2).

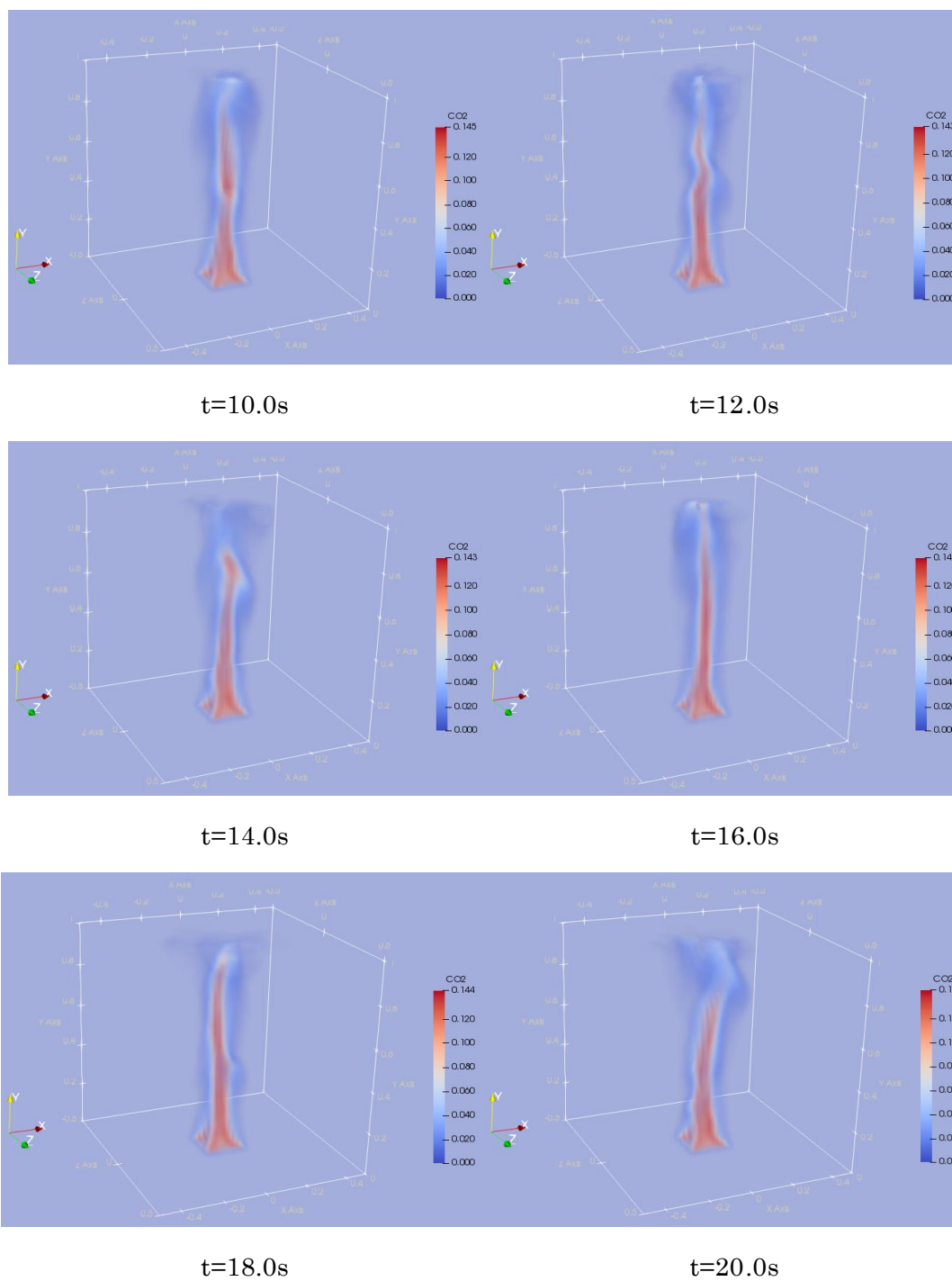


Fig.3.12 Distribution of carbon dioxide mass fraction in container A at t= 0.1, 0.5, 1.0, 4.0, 6.0, 8.0, 10.0, 12.0, 14.0, 16.0, 18.0, 20.0s (2/2).

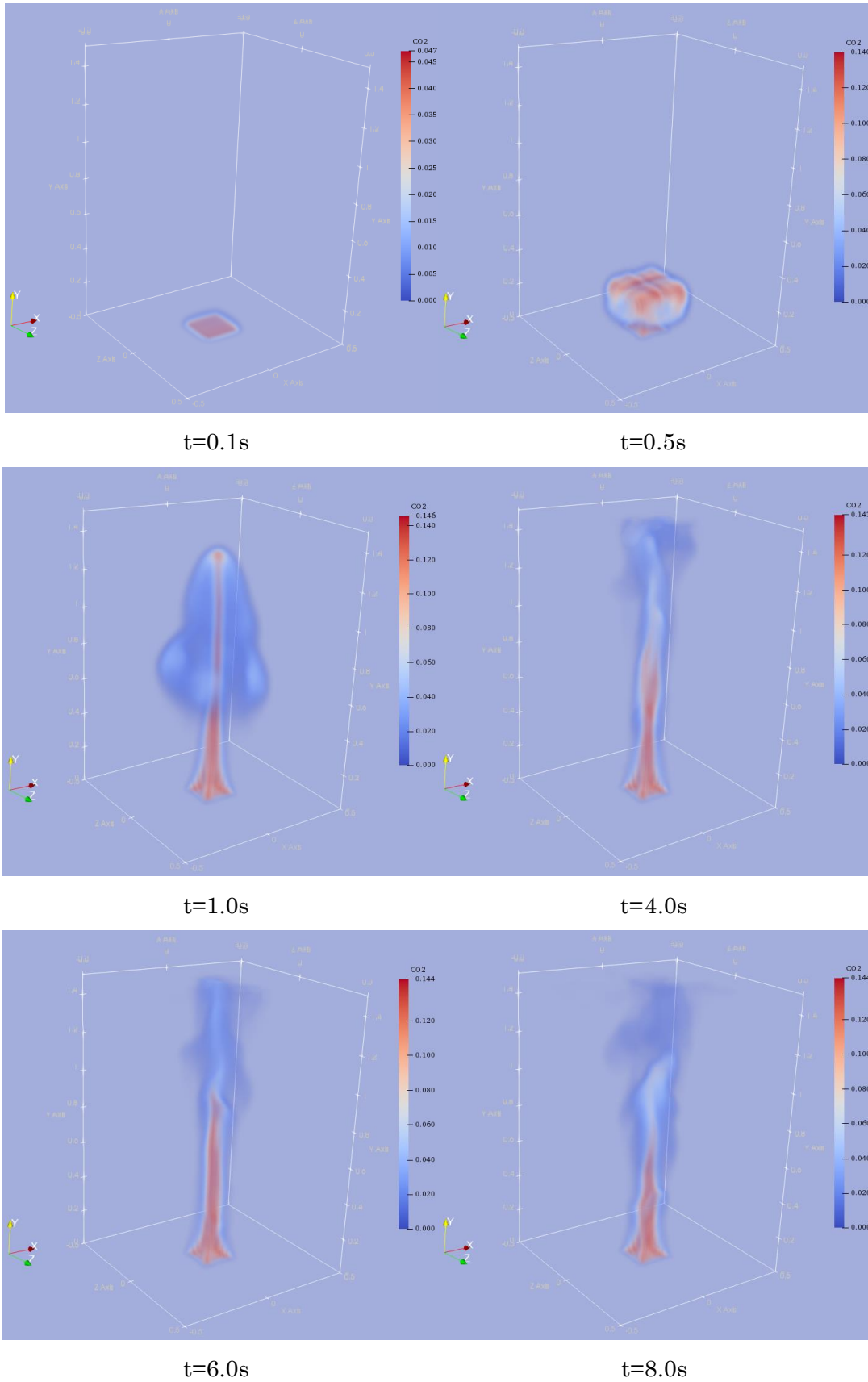


Fig.3.13 Distribution of carbon dioxide mass fraction in container B1 at  $t= 0.1, 0.5, 1.0, 4.0, 6.0, 8.0, 10.0, 12.0, 14.0, 16.0, 18.0, 20.0s$  (1/2).

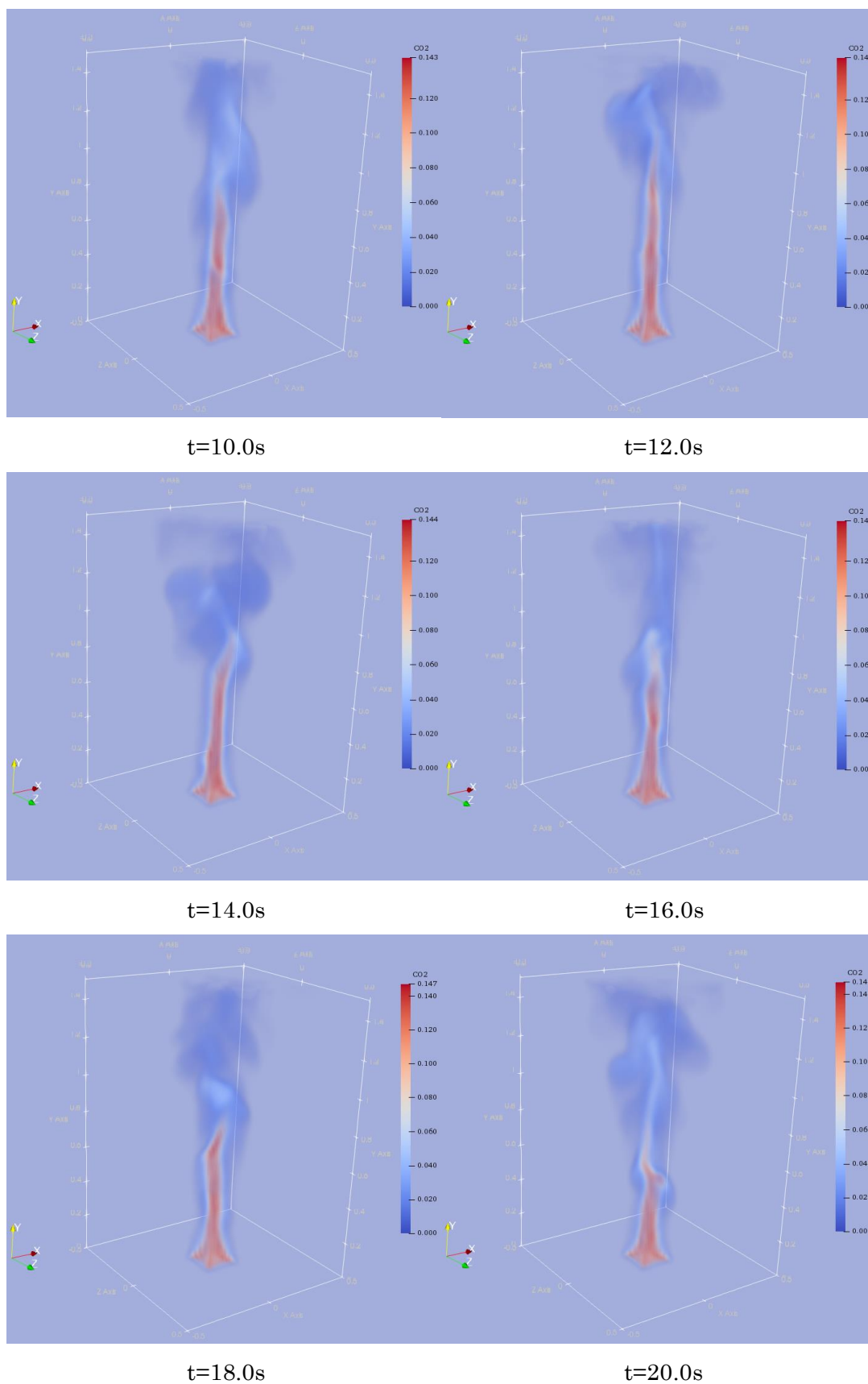


Fig.3.13 Distribution of carbon dioxide mass fraction in container B1 at t= 0.1, 0.5, 1.0, 4.0, 6.0, 8.0, 10.0, 12.0, 14.0, 16.0, 18.0, 20.0s (2/2).

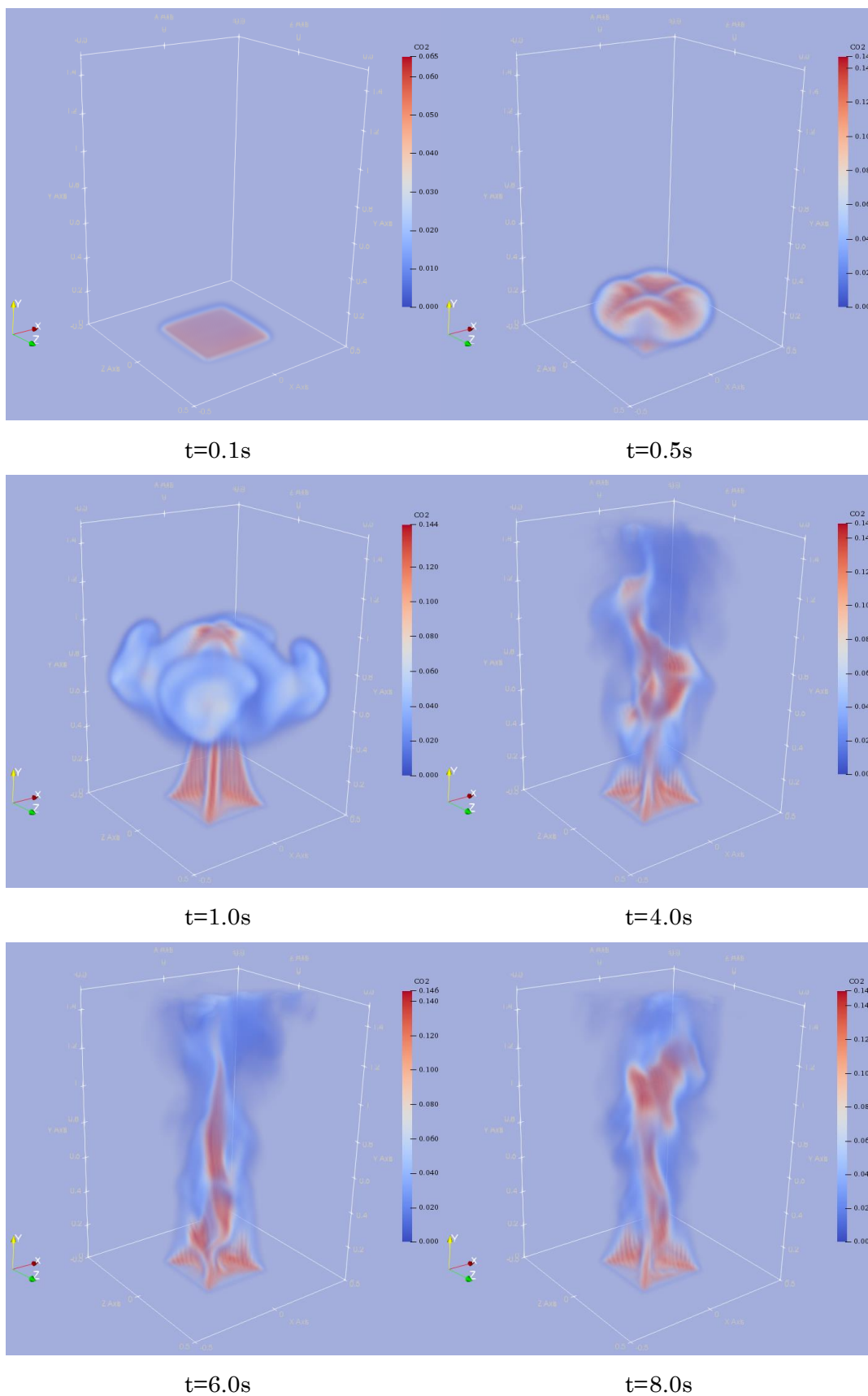


Fig.3.14 Distribution of carbon dioxide mass fraction in container B2 at  $t= 0.1, 0.5, 1.0, 4.0, 6.0, 8.0, 10.0, 12.0, 14.0, 16.0, 18.0, 20.0s$  (1/2).

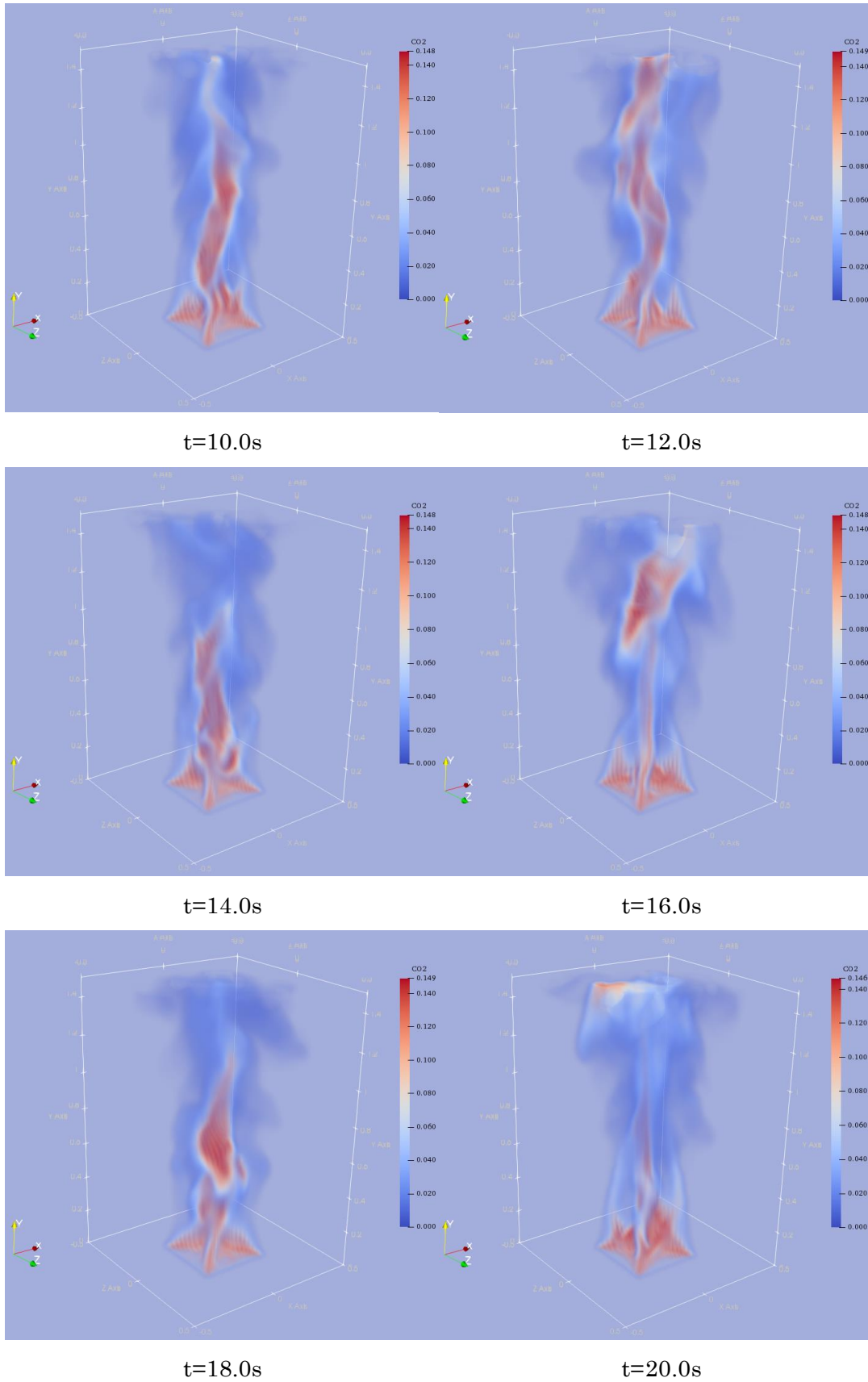


Fig.3.14 Distribution of carbon dioxide mass fraction in container B2 at t= 0.1, 0.5, 1.0, 4.0, 6.0, 8.0, 10.0, 12.0, 14.0, 16.0, 18.0, 20.0s (2/2).

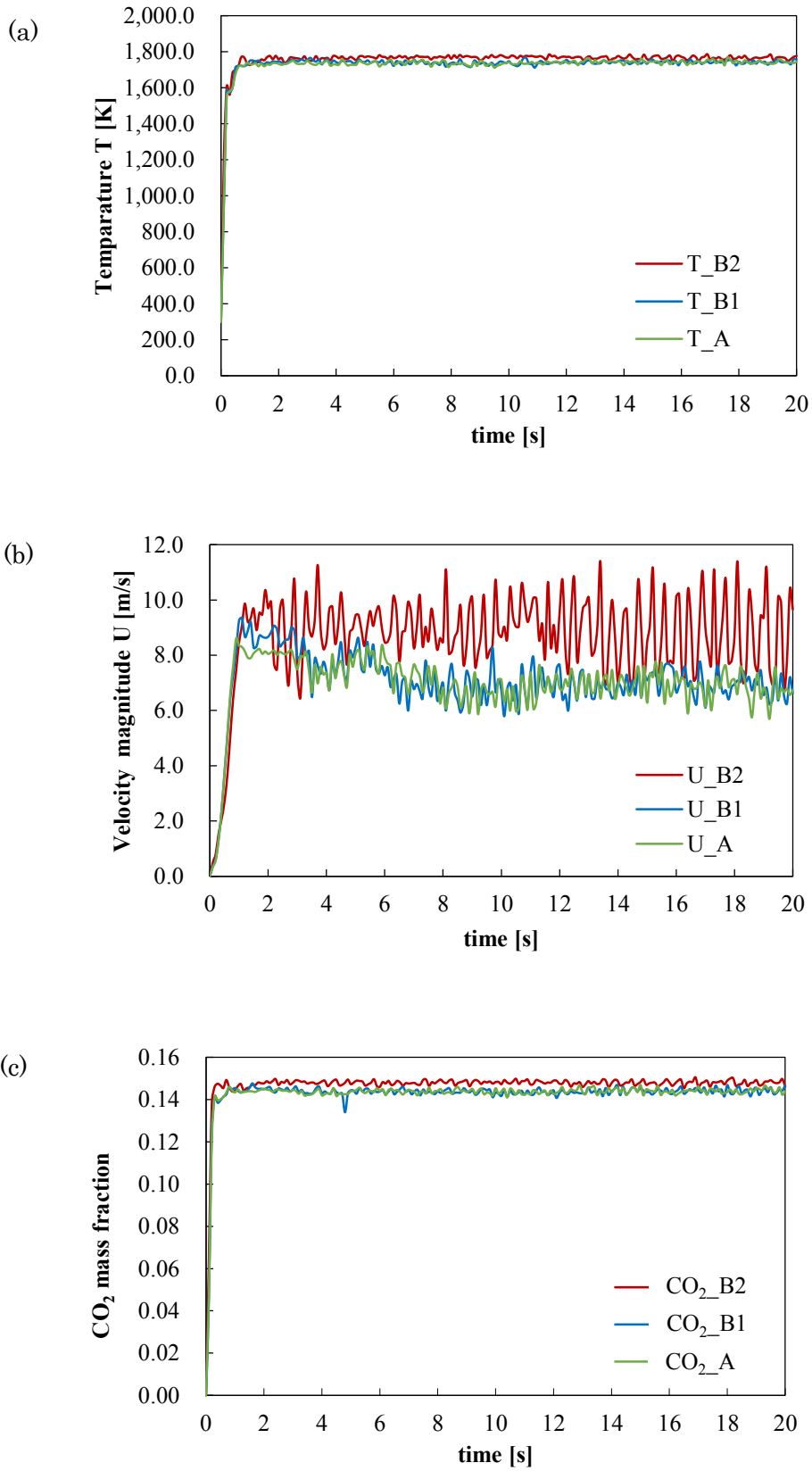


Fig.3.15 Time history of the maximum values of (a) temperature T [K], velocity magnitude U [m/s], and (c) CO<sub>2</sub> mass fraction at each output time step (0.1, 0.2, ..., 20).

### 3.7 Simulation of Gas Diffusion by FireFOAM Solver

We also used the FireFoam solver to study the diffusion behavior of methane, hydrogen and helium into air. Combustion process was set as activation false in combustionProperties. The size of the model is  $1.0\text{m} \times 1.0\text{m} \times 0.01\text{m}$  in  $x \times y \times z$  directions. The initial and boundary conditions for methane were set as the same conditions in the simulation with active combustion process. Transport properties for hydrogen and helium were taken from JANAF tables of thermodynamics. The inlet velocity was set to  $0.05\text{m/s}$  for each gas. For all simulations, the same time step interval ( $0.0001\text{s}$ ) and runtime  $10\text{s}$  were used. The obtained results for two dimensional simulation are shown in Fig.3.16 for methane, Fig.3.17 for hydrogen and Fig.3.18 for helium.

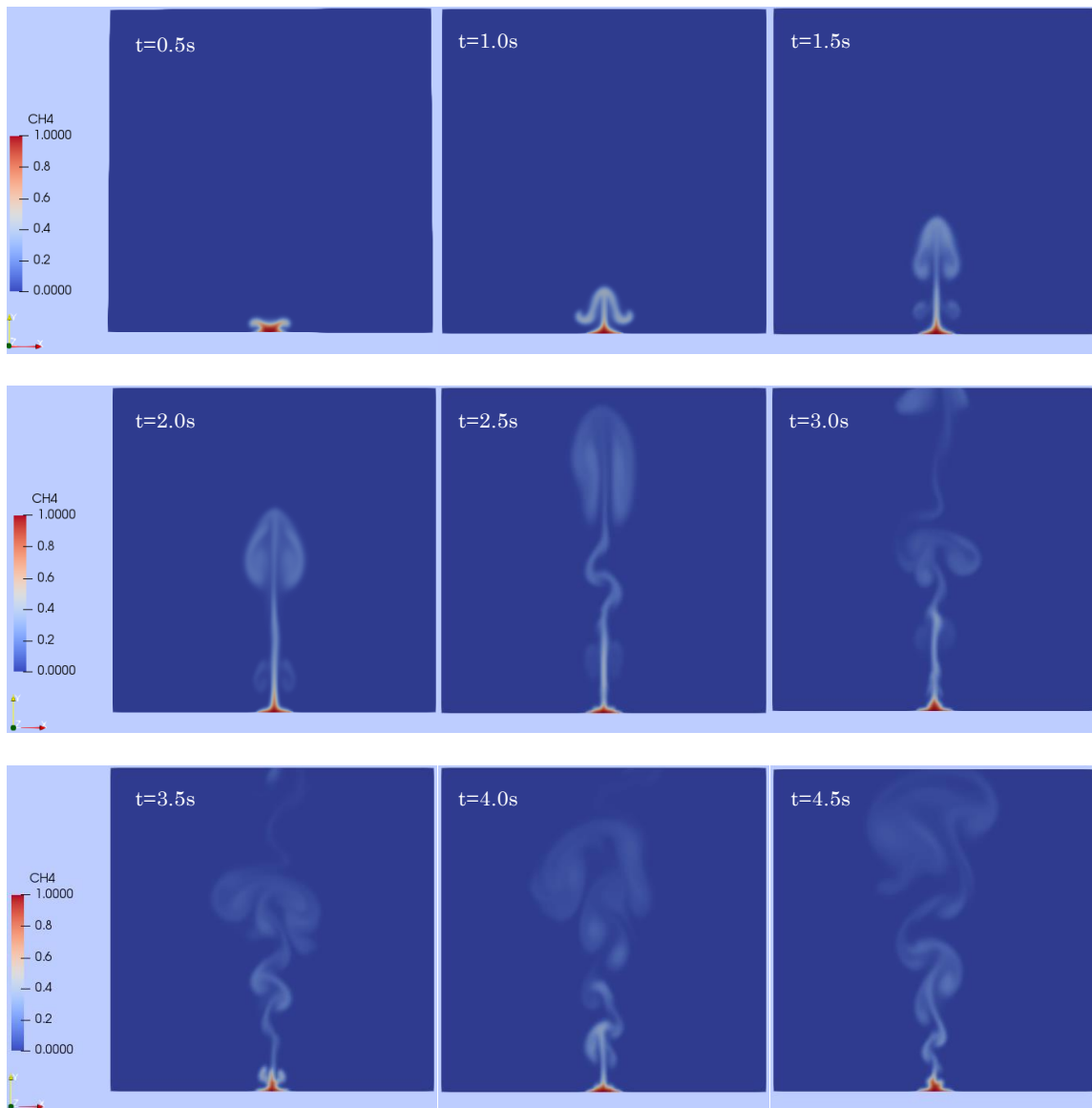


Fig.3.16 Diffusion behavior of methane into air at  $t= 0.5, 1.0, 1.5, 2.0, 2.5, 3.0, 3.5, 4.0, 4.5, 5.0, 5.5, 6.0, 6.5, 7.0, 7.5, 8.0, 8.5, 9.0, 9.5, 10.0\text{s}$  (1/2).

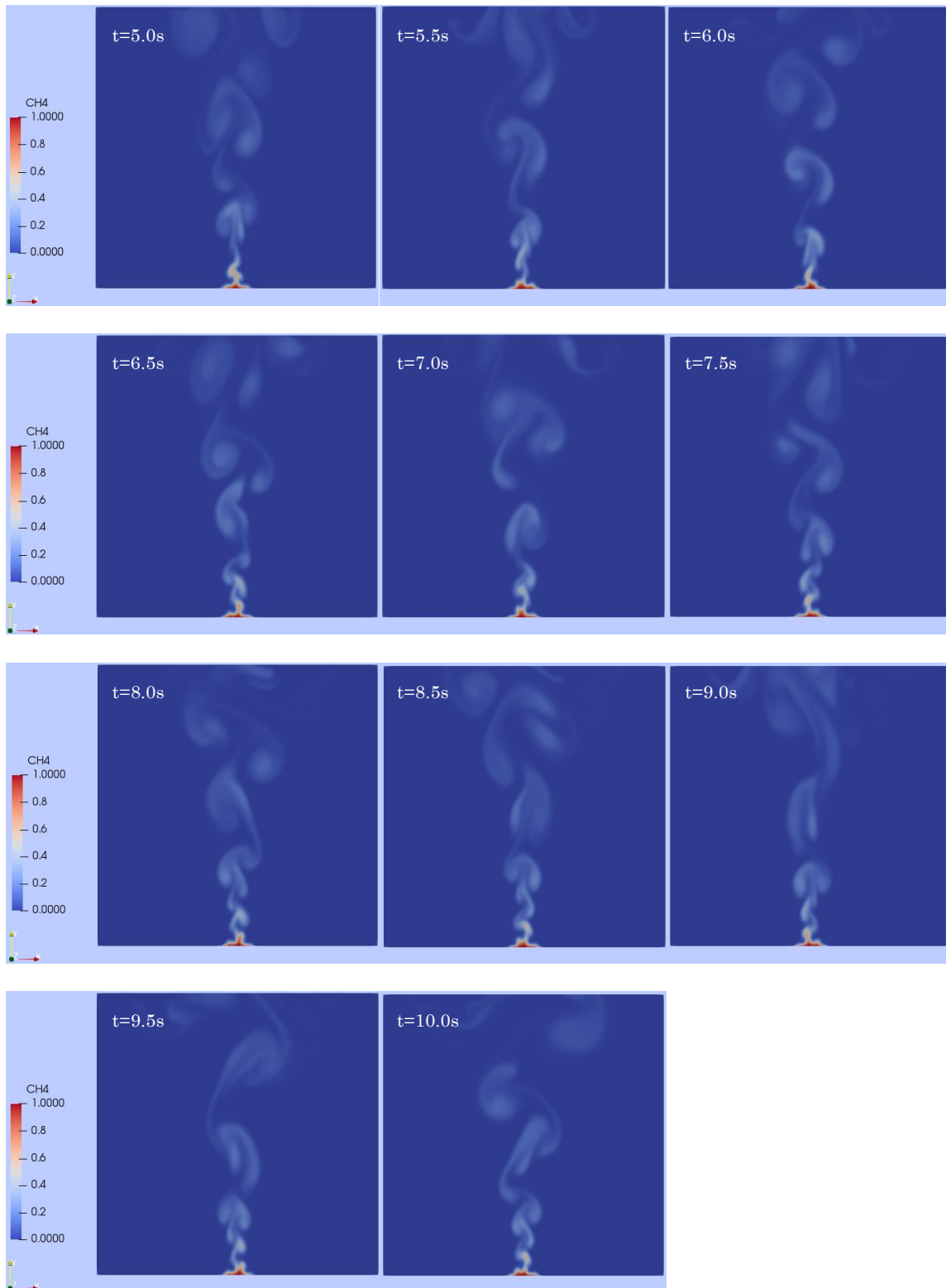


Fig.3.16 Diffusion behavior of methane into air at t= 0.5, 1.0, 1.5, 2.0, 2.5, 3.0, 3.5, 4.0, 4.5, 5.0, 5.5, 6.0, 6.5, 7.0, 7.5, 8.0, 8.5, 9.0, 9.5, 10.0s (2/2).

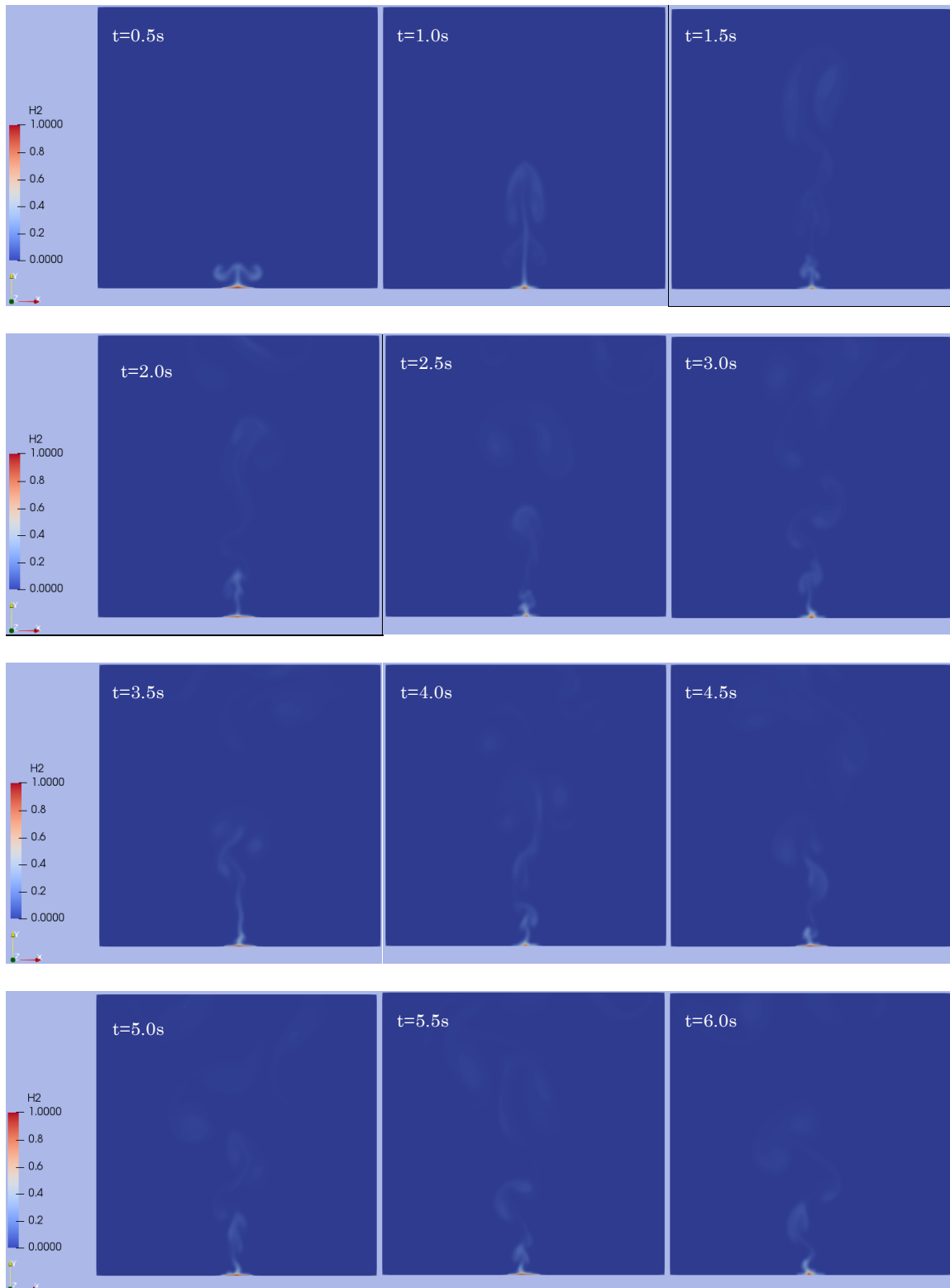


Fig.3.17 Diffusion behavior of hydrogen into air at  $t= 0.5, 1.0, 1.5, 2.0, 2.5, 3.0, 3.5, 4.0, 4.5, 5.0, 5.5, 6.0, 6.5, 7.0, 7.5, 8.0, 8.5, 9.0, 9.5, 10.0\text{s}$  (1/2).

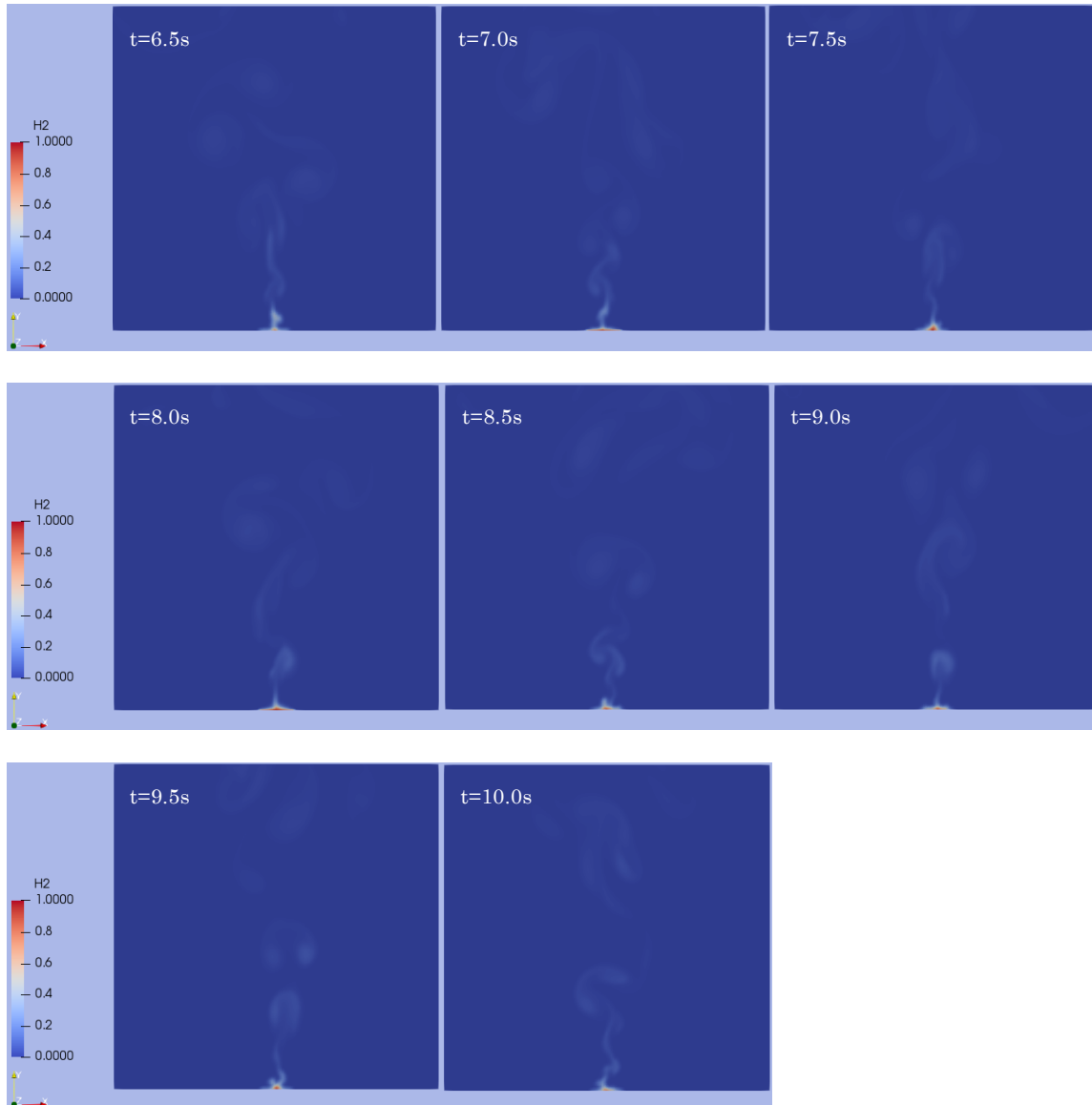


Fig.3.17 Diffusion behavior of hydrogen into air at t= 0.5, 1.0, 1.5, 2.0, 2.5, 3.0, 3.5, 4.0, 4.5, 5.0, 5.5, 6.0, 6.5, 7.0, 7.5, 8.0, 8.5, 9.0, 9.5, 10.0s (2/2).

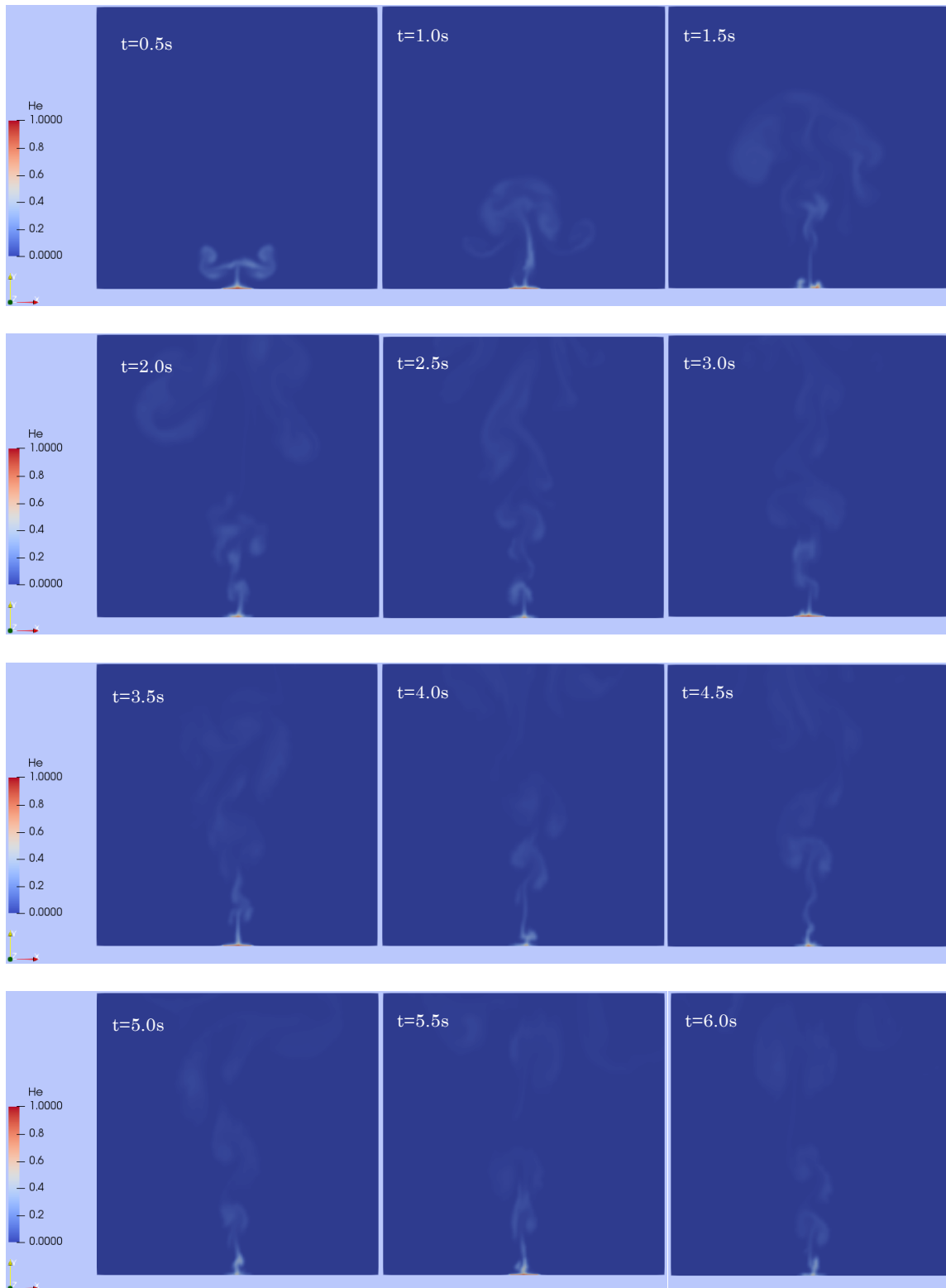


Fig.3.18 Diffusion behavior of helium into air at  $t= 0.5, 1.0, 1.5, 2.0, 2.5, 3.0, 3.5, 4.0, 4.5, 5.0, 5.5, 6.0, 6.5, 7.0, 7.5, 8.0, 8.5, 9.0, 9.5, 10.0s$  (1/2).

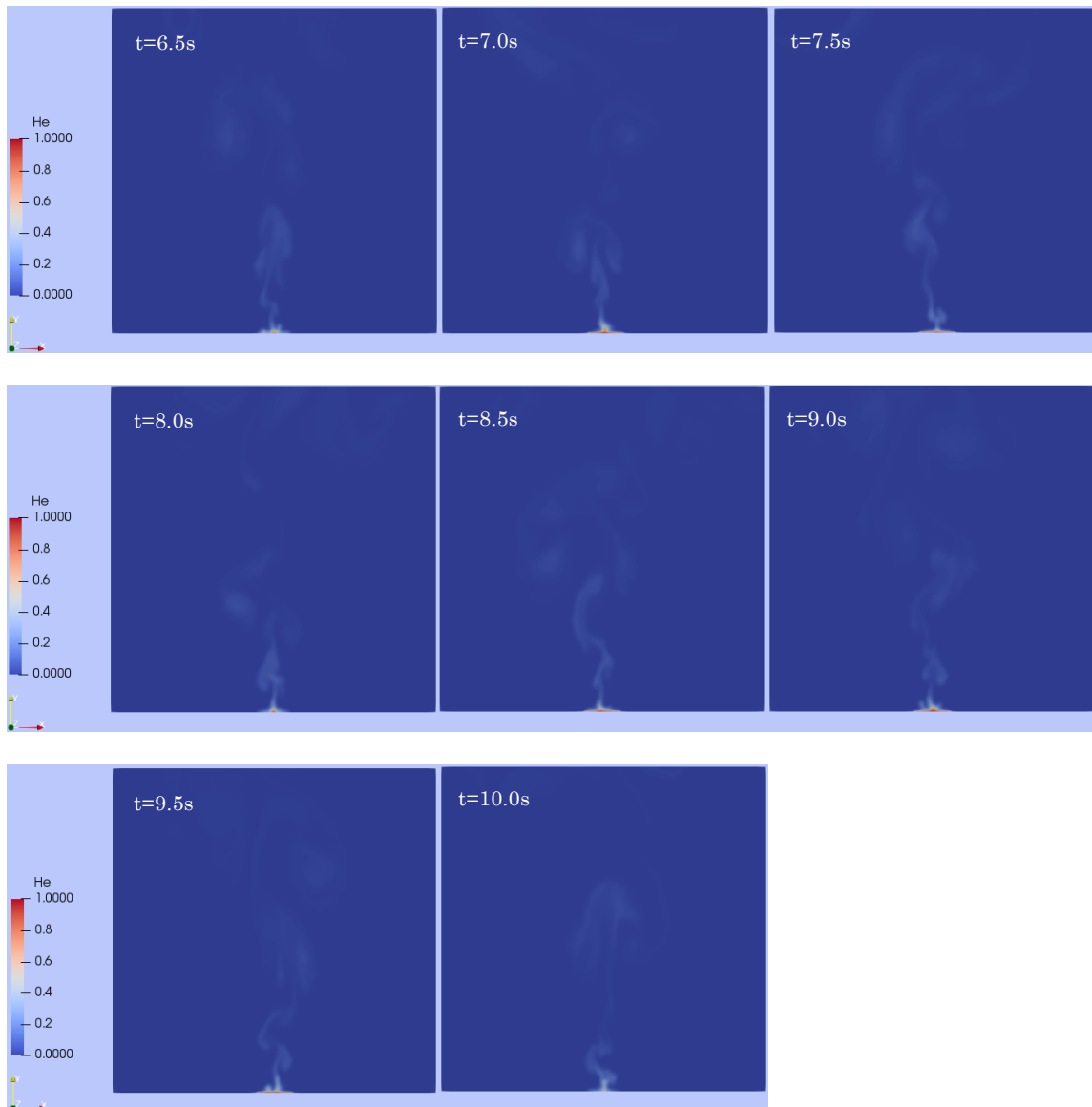


Fig.3.18 Diffusion behavior of helium into air at t= 0.5, 1.0, 1.5, 2.0, 2.5, 3.0, 3.5, 4.0, 4.5, 5.0, 5.5, 6.0, 6.5, 7.0, 7.5, 8.0, 8.5, 9.0, 9.5, 10.0s (2/2).

The obtained results show that helium diffused faster than hydrogen and methane into the air. According to the Ref.[17], considering the combination of the effects of mass and size of helium atom and hydrogen molecules, hydrogen molecule might diffuse 1.1 times faster than helium atom at the same temperature and pressure. However, helium diffuses and leaks faster than hydrogen through solids, and small cracks or holes as helium atom is smaller than hydrogen molecules. Thus, the results from current simulations by FireFoam solver are consistent with the Ref.[17]. By generating the vector glyph for velocity of each gas in paraView, the difference in diffusion behaviors can be seen as in Fig.3.19 (t= 1.0, 2.0 and 4.0s).

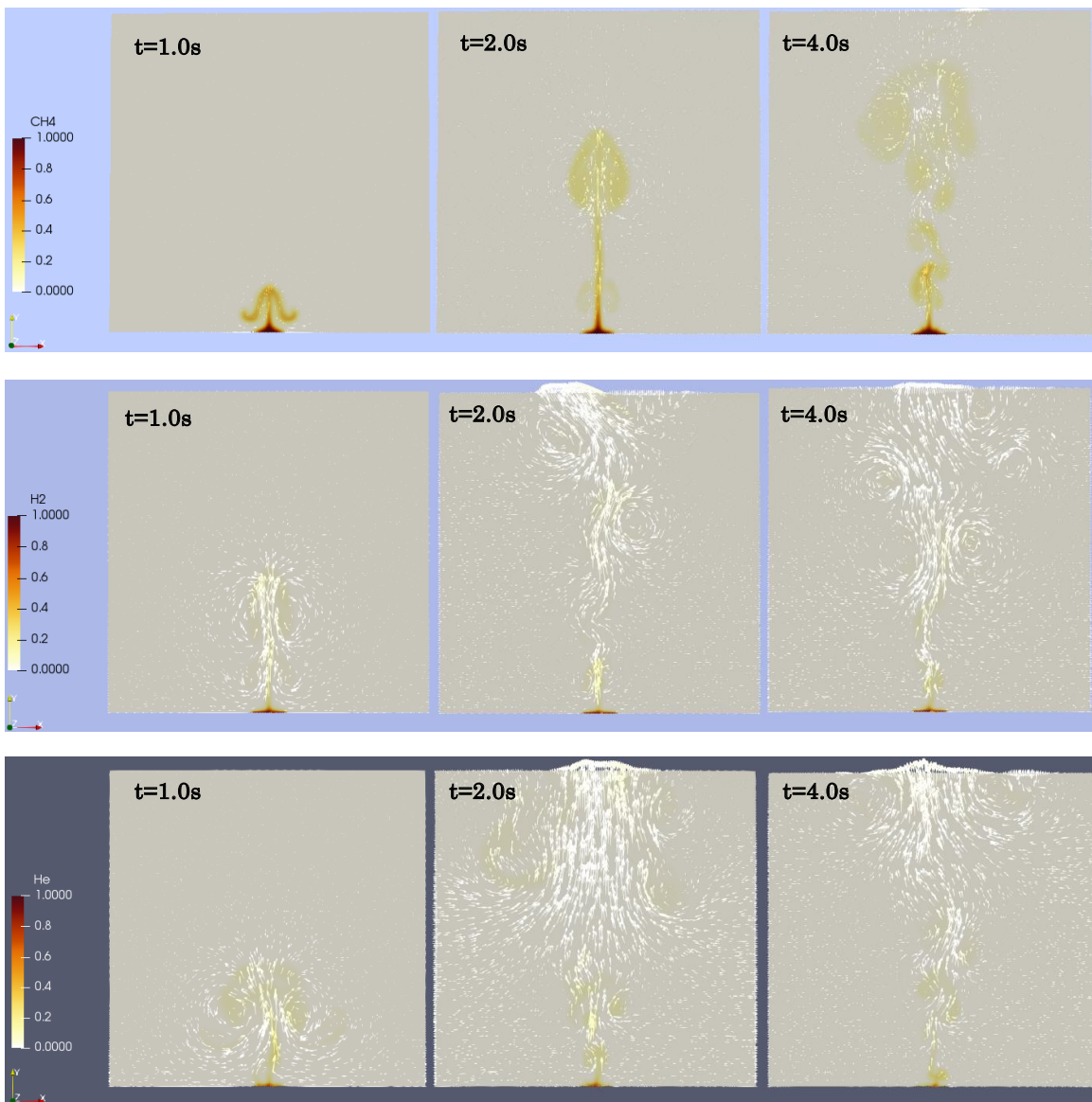


Fig.3.19 Comparison of the diffusion of methane, hydrogen and helium into air by FireFoam solver.

## 4. Preliminary Numerical Simulation by XiFOAM Solver

### 4.1 Case Setup for Hydrogen-Air Combustion

In this case we considered the premixed combustion of hydrogen-air in cubic combustion vessel based on the case in which released hydrogen gas is mixed with exiting air in the radioactive waste vessel. XiFoam is the solver for compressible premixed/partially-premixed combustion with turbulence modelling. To save computational time, one-eighth of the vessel with the size of  $0.26\text{m} \times 0.26\text{m} \times 0.26\text{m}$  in  $x \times y \times z$  direction was used as geometry model. The skeletal of the case file is as follow:

Case__		
__0 time directory	__constant	__system
_alphat	_combustionProperties	_blockMeshDict
_b	_thermophysicalProperties	_controlDict
_epsilon	_turbulenceProperties	_fvSchemes
_ft		_fvSolution
_fu		
_k		
_nut		
_p		
_S <sub>u</sub>		
_T		
_T <sub>u</sub>		
_U		
_Xi		

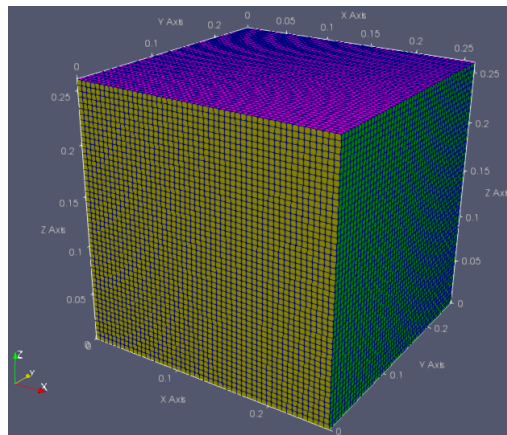


Fig. 4.1 Mesh configuration of the one-eighth of combustion vessel.

Mesh generating was performed by *blockMesh* with simple grading (uniform grid size) in all dimensions and the number of cell is 125000. The generated model is shown in Fig.4.1.

#### 4.2 Initial and Boundary Conditions

For numerical simulation, initial temperature, pressure and laminar burning velocity were set as 300K,  $1.01325 \times 10^5$  Pa and  $2.446 \text{ms}^{-1}$ , respectively. For all boundaries, boundary field type was set as *symmetryPlane*, and internal field was set up as in Table 4.1. the values for *alphat*, *b*, *epsilon*  $\epsilon$ , *ft*, *fu*, *k* and *nut* were set as default values of OpenFOAM.

Table 4.1 Parameter setup for internal fields.

<i>alphat</i>	0	$\text{kgm}^{-1}\text{s}^{-1}$
<i>b</i>	1	-
$\epsilon$	375	$\text{m}^2\text{s}^{-3}$
<i>ft</i>	0.06	-
<i>fu</i>	0	-
<i>k</i>	1.5	$\text{ms}^{-2}$
<i>nut</i>	0	$\text{ms}^{-1}$
<i>p</i>	$1.01325 \times 10^5$	Pa
$S_u$	2.446	$\text{ms}^{-1}$
<i>T</i>	300	K
$T_u$	300	K
<i>U</i>	0	$\text{ms}^{-1}$
<i>Xi</i>	1	-

#### 4.3 Numerical Simulation

The progress variable, *c*, which serve as a basic parameter in premixed combustion is obtained by the following equation

$$c = 1 - b$$

where *b* is the density-weighted mean reaction regress variable. The value of *c* varies across the flame from 0 (unburned gas) to 1.0 (burned gas) by showing the progress of reaction. The transport equation used in the modelling of flame front propagation with *b* in XiFoam is as follow:

$$\frac{\partial}{\partial t}(\rho b) + \nabla \cdot (\rho \vec{u} b) - \nabla \cdot \left( \frac{\mu_t}{S_{ct}} \nabla b \right) = -\rho_u S_u Xi |\nabla b|$$

where,  $S_u$  is the laminar flame speed, *Xi* (flame wrinkling factor) is the ratio of turbulent flame velocity to laminar flame velocity ( $S_t/S_u$ ),  $S_{ct}$  is the turbulent Schmidt number,  $\mu_t$  is the turbulent viscosity and  $\rho_u$  is the density of unburned mixture.

The value  $Xi$  is calculated by the following algebraic equations,

$$Xi_{eq} = 1 + 2(1-b)(Xi_{eq}^* - 1)$$

$$Xi_{eq}^* = 1 + 0.62 \sqrt{\frac{u'}{S_u}} R_\eta$$

where,  $u'$  is the turbulence intensity,  $R_\eta$  is the Kolmogorov Reynolds number.

There are three types of model for laminar flame speed calculations: (1) unstrained (2) algebraic and (3) transport. In this simulation, SuModel was chosen as unstrained. Flame propagation radius which is one of the important parameter in turbulent premixed combustion is measured by implementing the following equation [14] in default XiFoam solver.

$$R = \left[ \left( \frac{3}{4\pi\rho_b} \iiint \rho(1-b) dx dy dz \right) \right]^{1/3}$$

where  $\rho_b$  is the minimum density of burned gas.

Ignition site was located at the centre of combustion vessel (0.0005 0.0005 0.0005) and duration of ignition was 0.003s. The equivalence ratio was set to 1.0. Gulderson formulation for laminar flame speed of specific fuel is the default equation in XiFoam to calculate  $S_u$ . The transport equation is as follow:

$$S_u = W \phi^\eta \exp[-\xi(\phi - 1.075)^2] \left(\frac{T}{T_0}\right)^\alpha \left(\frac{p}{p_0}\right)^\beta$$

where  $W$ ,  $\eta$ ,  $\xi$ ,  $\alpha$  and  $\beta$  are Gulderson coefficients.  $\phi$  is the equivalence ratio.

The composition of the fuel and air and initial laminar flame speed were taken from the data by UCSD mechanism developed by the San Diego University [15].

The thermoPhysical model was chosen as `heheuPsiThermo>homogeneousMixture>const>janaf>perfectGas>specie>absoluteEnthalpy`. RAS (Reynolds-Averaged Simulation) turbulence model was applied for simulation. PIMPLE algorithm which is the combination of PISO (Pressure Implicit with Splitting of Operator) and SIMPLE (Semi-Implicit Method for Pressure-Linked Equations), was used in the XiFoam solver. Time step interval was  $5 \times 10^{-6}$  and computational runtime was 0.01s.

#### 4.4 Results and Discussion

The flame propagation sustains after the ignition period (0.003s) since the ignition strength, i.e. ignition energy, was set to 3 in `combustionProperties`. Figure 4.2 shows the temperature distribution at  $t=0.001s$  to  $0.01s$ . The obtained burned gas temperature 2644.4438K at  $t=0.01s$  is smaller than the temperature of 2766K which is obtained by constant volume combustion for stoichiometric hydrogen-air [16]. The distribution of

turbulent flame speed and laminar flame speed are shown in Fig.4.3 and Fig.4.4, respectively. The maximum value of temperature and pressure through the domain depending on time are plotted in Fig.4.5. Figure 4.6 shows the flame wrinkling factor, turbulent flame speed and laminar flame speed. Flame propagation radius, R is compared with the experimental results obtained by Kadowaki et al. [18] and plotted in Fig.4.7.

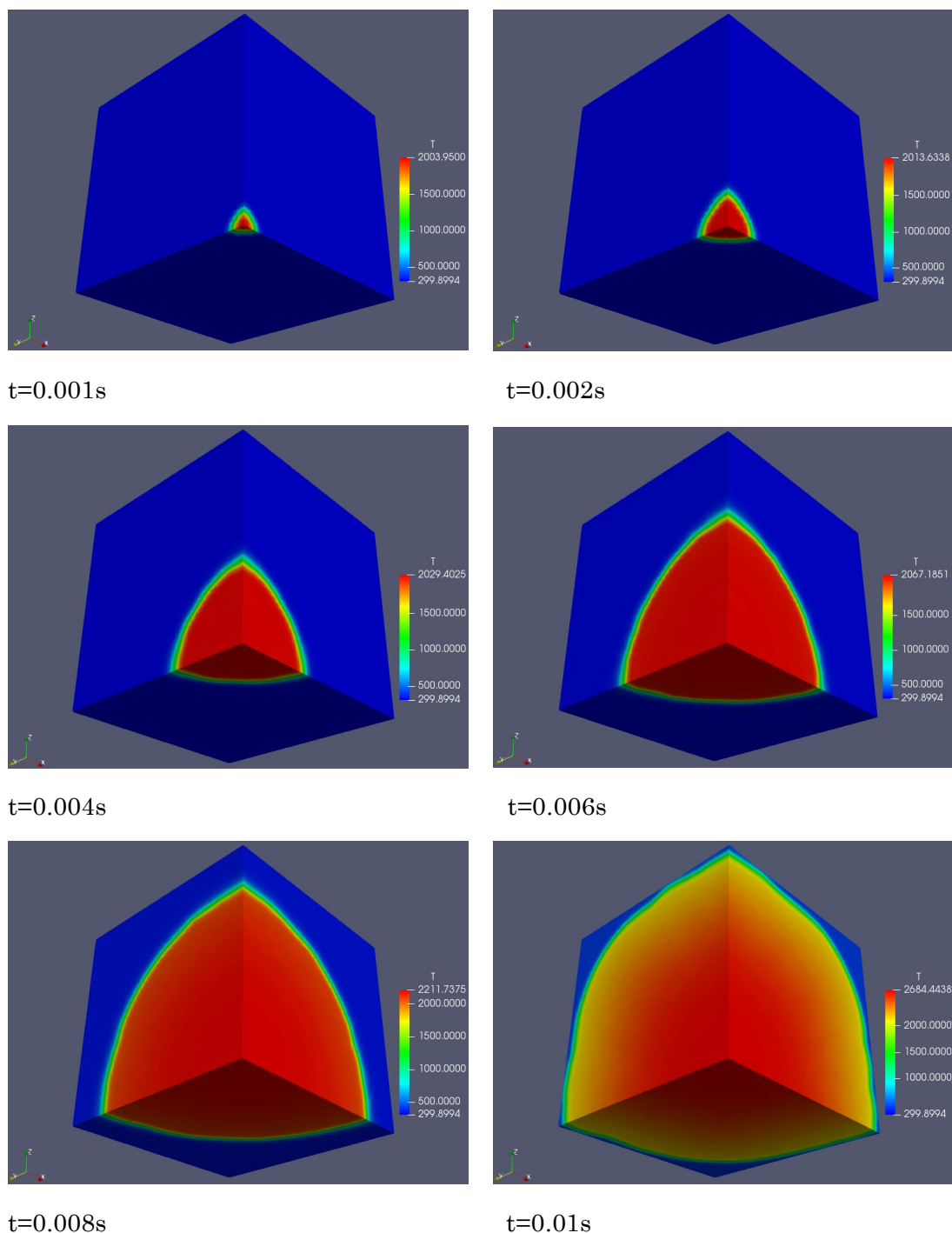


Fig.4.2 Temperature distribution of H<sub>2</sub>-air premixed flame ( $\phi = 1.0$ ) at 0.001, 0.002, 0.004, 0.006, 0.008, 0.01s.

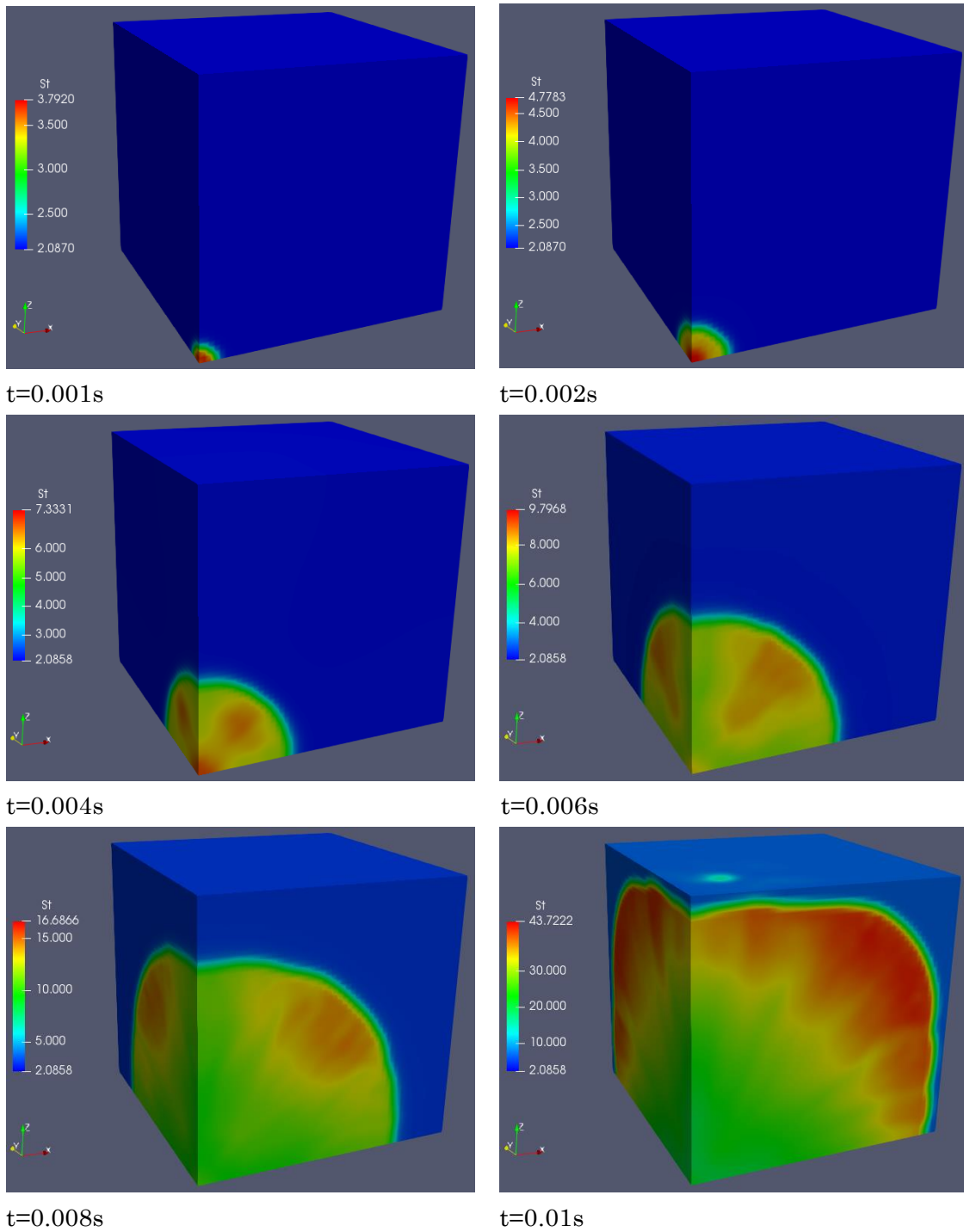


Fig.4.3 Distribution of turbulent flame speed of H<sub>2</sub>-air premixed flame ( $\phi = 1.0$ ) at 0.001, 0.002, 0.004, 0.006, 0.008, 0.01s.

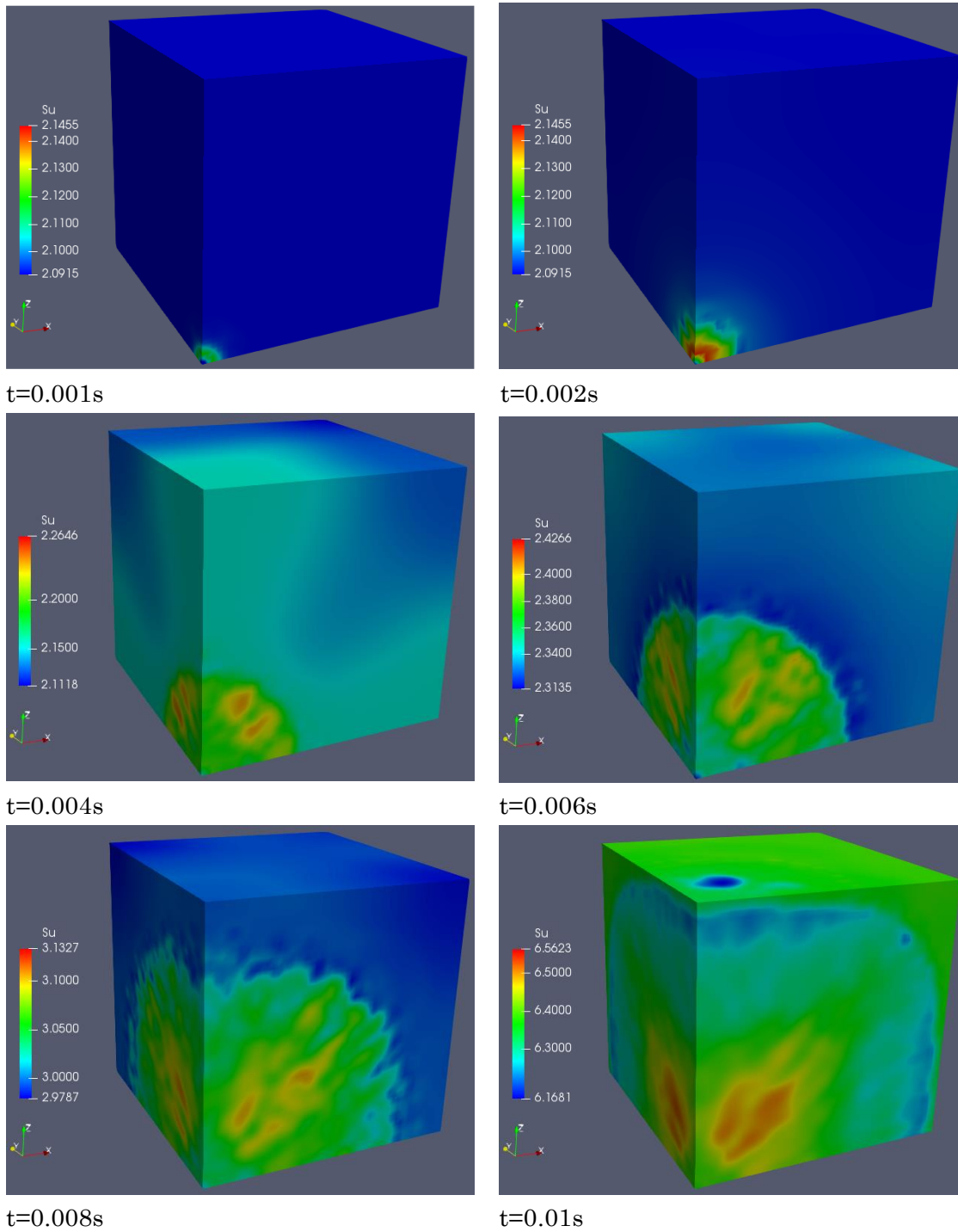


Fig.4.4 Distribution of laminar flame speed of  $H_2$ -air premixed flame ( $\phi=1.0$ ) at 0.001, 0.002, 0.004, 0.006, 0.008, 0.01s.

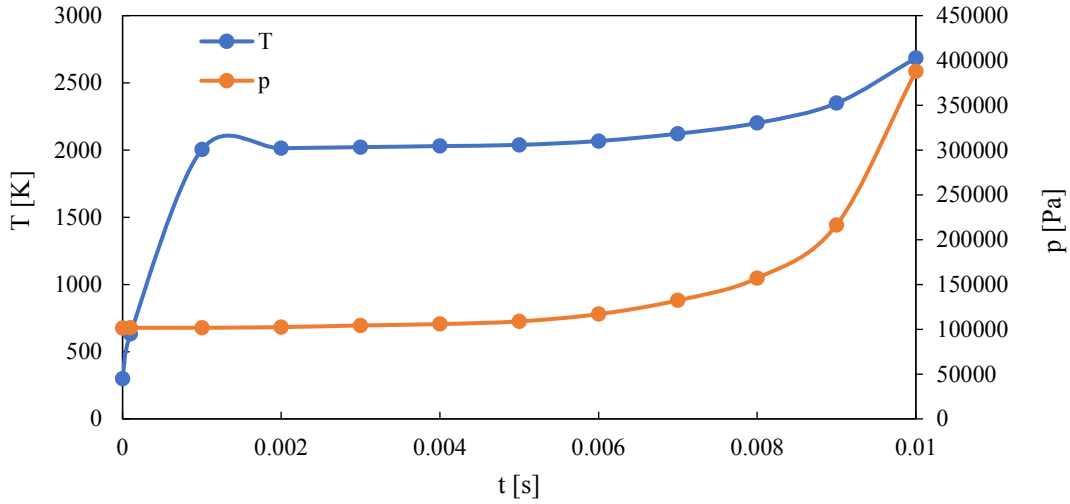


Fig. 4.5 Burned-gas temperature and pressure of H<sub>2</sub>-air premixed flame ( $\phi = 1.0$ ).

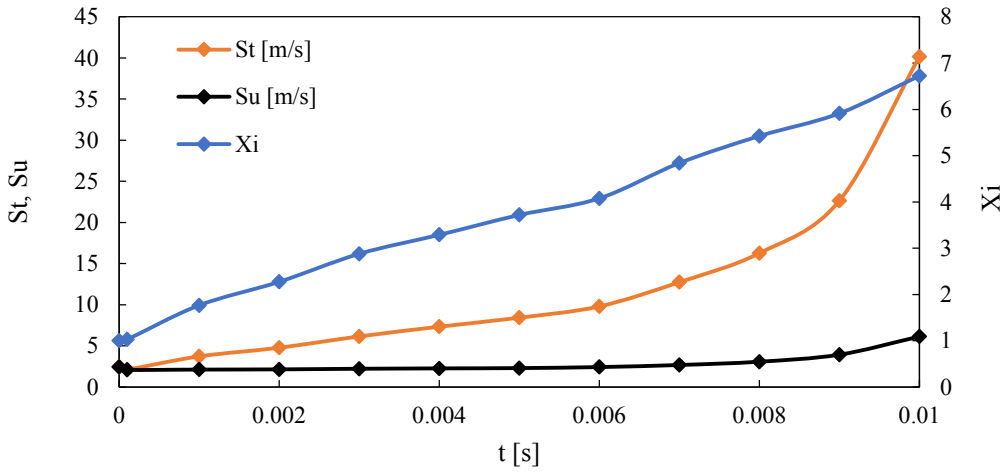


Fig. 4.6 Flame wrinkling factor, turbulent flame speed and laminar flame of H<sub>2</sub>-air premixed flame ( $\phi = 1.0$ ).

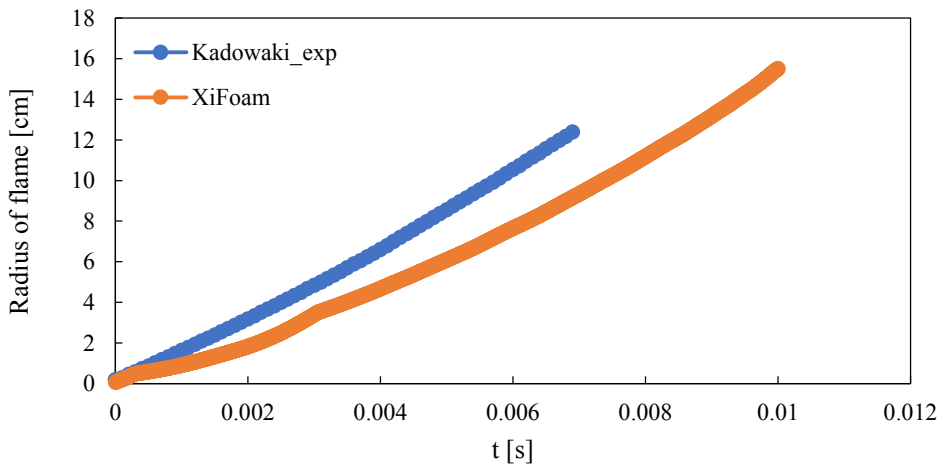


Fig. 4.7 Flame propagation radius of H<sub>2</sub>-air premixed flame ( $\phi = 1.0$ ).

## 5. Concluding Remarks

We performed this numerical simulation in order to (1) understand the behaviors and characteristics of methane combustion in the container which was supported by default FireFOAM, as the preliminary step to continue the study of behavior and characteristics of hydrogen combustion and explosion in nuclear waste vessel/container, and (2) be familiar with the usage of solvers and utilities of OpenFOAM together with the visualization tool ParaView for combustion and explosion regimes. By using open source application, the computational cost for numerical simulation may be reduced in large computational size of domain and long computational time in parallel compilations compared with the commercial tools.

In the first case, we used simple rectangular container with the fuel inlet at the base where the fuel was sinking or entering. As the results, when the height of container increased and inlet size became larger, the average temperature increased along with the vigorous distribution, and average burning velocity and generation of carbon dioxide increased. These results indicated that the size of container and inlet affected the behavior and characteristics of combustion.

In this simulation, the container was set to be opened in outlet side. To understand the actual combustion and explosion phenomena, we need to set close type one. For different types of nuclear wastes, various types of nuclear wastes canisters are in different shapes and sizes which are kept in vessel/container or on the surface ground or in the under-ground system. Thus, we need to prepare various geometries and sizes in the next simulations. In addition, as the concentration of accumulated gas varies depending on the types of nuclear waste and canister, simulations for different levels of hydrogen concentration need to be considered.

The simulation of the diffusion behaviors of methane, hydrogen and helium were also performed by FireFoam solver. The obtained results showed that helium diffused faster than hydrogen and methane.

In the second case, numerical simulation of the combustion of premixed hydrogen-air under the stoichiometric conditions in the cubic combustion chamber based on the case in which released hydrogen gas is mixed with exiting air in the waste vessel was performed by XiFoam solver. The flame propagation sustained after the ignition period. The obtained burned gas temperature is smaller than the temperature obtained by constant volume combustion of H<sub>2</sub>-air. The radius of flame propagation was obtained and compared with the experimental results of Kadowaki et al. The current results by XiFoam are smaller than experimental results. This shows that simulation results by OpenFoam solver strongly depends on setup parameter and the choice of models in combustion and transport properties.

To meet the various required conditions, OpenFOAM source codes for specific solvers that will be chosen in our simulations have to be modified. We need to apply other combustion standard solvers such as reactingFoam, rhoReactingFoam, and ddtFoam which is an additional solver to OpenFOAM and specialized for deflagration to detonation regimes in combustion, besides the fireFoam. So that the most relevant solver will be come out for combustion of hydrogen in waste vessel. To complete the simulations, we also need other application tools to create complex geometries and generate mesh, and to perform the calculations for thermochemical data of hydrogen that will be used in simulation as initial conditions. In the next simulations, methane will be substituted with hydrogen as the second step to approach to our research objectives.

## References

- [1] A. Bentaib, N. Meynet, and A. Bleyer, Overview on hydrogen risk research and development activities: methodology and open tissues, *Nuclear Engineering and Technology*, vol. 47, no.1, pp.26-32 (2015).
- [2] J.O. Liljenzin and J. Rydberg, Risk from Nuclear Waste, ISSN 1104-1374, ISRN SKI-R—96/70-SE (1996), available from <http://www.iaea.org/inis/collection/NCICollectionStore/Public/28/028/28028626.pdf> (accessed 2018-06-12).
- [3] J. Pritrsky, I. Matejovic, F. Ondra and V. Necas, Assessment of gas producing radioactive waste disposal, *Journal of Electrical Engineering*, vol.57, no.4, pp.235-237 (2006).
- [4] C.W. Stewart, S.A. Hartley, P.A. Meyer and B.E. Wells, Predicting peak hydrogen concentration from spontaneous gas releases in Hanford waste tanks, Pacific Northwest National Laboratory (2005), available from [https://www.pnnl.gov/main/publications/external/technical\\_reports/PNNL-15238.pdf](https://www.pnnl.gov/main/publications/external/technical_reports/PNNL-15238.pdf) (accessed 2018-05-24).
- [5] B.L. Anderson, M.K. Sheaffer and L.E. Fisher, Hydrogen generation in TRU waste transportation packages, Lawrence Livermore National Laboratory (2000), available from <https://www.nrc.gov/docs/ML0037/ML003723404.pdf> (accessed 2018-06-19).
- [6] D.T. Hobbs, P.W. Norris, S.A. Pucko, N.E. Bibler, D.D. Walker and P.D. d'Entremont, Hydrogen generation rates in SAVANNAH river site high-level nuclear waste, *INIS*, vol.23, no.17, pp.1063-1066 (1992).
- [7] J.S. Small, M. Nykyri, M. Vikman, M. Itavaara, L. Heikinheimo, The biogeochemistry of gas generation from low-level nuclear waste: Modelling after 18 years study under in situ conditions, *Applied Geochemistry*, vol.84, pp.360-372 (2017).
- [8] The open source CFD toolbox, available from <http://www.openfoam.com/> (accessed 2018-04-16)  
<https://cfd.direct/openfoam/features/> (accessed 2018-04-16)  
<https://www.openfoam.com/documentation/user-guide/> (accessed 2018-04-16).
- [9] ParaView, available from <http://www.paraview.org> (accessed 2018-04-16).
- [10] Bjarne Husted, Ying Zhen Li, Chen Huang, Johan Anderson, Robert Svensson, Haukur Ingason, Marcus Runefors, and Jonathan Wahlqvist, Verification, validation and evaluation of FireFOAM as a tool for performance based design (2017), available from [https://www.brandskyddsforeningen.se/globalassets/brandforsk/rapporter-2017/brandforsk\\_rapport\\_309\\_131\\_firefoam\\_new.pdf](https://www.brandskyddsforeningen.se/globalassets/brandforsk/rapporter-2017/brandforsk_rapport_309_131_firefoam_new.pdf) (accessed 2018-06-28).
- [11] The open source CFD toolbox, Standard boundary conditions, available from <https://www.openfoam.com/documentation/user-guide/standard-boundaryconditions.php> (accessed 2018-05-15).
- [12] C.A. Sedano, O.D. Lopez, A. Ladino, and F. Munoz, Prediction of a small-scale pool fire with FireFoam, *Hindawi, International Journal of Chemical Engineering*, vol.2017,

Article ID 4934956, available from <https://doi.org/10.1155/2017/4934956>  
(accessed 2018-06-28).

- [13] DDTFoam, available from <http://sourceforge.net/projects/ddtfoam> (accessed 2018-07-06).
- [14] Ehsan Yasari, Tutorial XiFoam (2010), available from [http://www.tfd.chalmers.se/~hani/kurser/OS\\_CFD\\_2010/ehsanYasari/ehsanYasariReport.pdf](http://www.tfd.chalmers.se/~hani/kurser/OS_CFD_2010/ehsanYasari/ehsanYasariReport.pdf) (accessed 2018-07-06).
- [15] Cantera User's Guide, Hydrogen/Air Combustion, available from <https://www.cerfacs.fr/cantera/mechanisms/hydro.php> (accessed 2018-07-06).
- [16] A.E. Dahoe, Laminar burning velocities of hydrogen-air mixtures form closed vessel gas explosions, *Journal of Loss Prevention in the Process Industries*, vol.18, pp.152-166 (2005).
- [17] Does helium diffuse faster than hydrogen?, <https://www.quora.com/Does-helium-diffuse-faster-than-hydrogen> (accessed 2018-08-22).
- [18] 平成 26 年度発電用原子炉等安全対策高度化技術基盤整備事業, 水素安全対策高度化, 事業報告書, pp.401-407 (H.27).

## Appendix

```
// controlDict..... //
application      fireFoam;
startFrom        latestTime;
startTime        0.0;
stopAt           endTime;
endTime          20.0;
deltaT           0.0001;
writeControl     adjustableRunTime;
writeInterval    0.1;
purgeWrite       0;
writeFormat      binary;
writePrecision   6;
writeCompression off;
timeFormat       general;
timePrecision    6;
graphFormat      raw;
runTimeModifiable yes;
adjustTimeStep   yes;
maxCo            0.6;
maxDeltaT        0.1;
```

This is a blank page.

# 国際単位系 (SI)

表1. SI 基本単位

基本量	SI 基本単位	
	名称	記号
長さ	メートル	m
質量	キログラム	kg
時間	秒	s
電流	アンペア	A
熱力学温度	ケルビン	K
物質량	モル	mol
光度	カンデラ	cd

表2. 基本単位を用いて表されるSI組立単位の例

組立量	SI 組立単位	
	名称	記号
面積	平方メートル	m <sup>2</sup>
体積	立方メートル	m <sup>3</sup>
速度	メートル毎秒	m/s
加速度	メートル毎秒毎秒	m/s <sup>2</sup>
波数	毎メートル	m <sup>-1</sup>
密度, 質量密度	キログラム毎立方メートル	kg/m <sup>3</sup>
面積密度	キログラム毎平方メートル	kg/m <sup>2</sup>
比体積	立方メートル毎キログラム	m <sup>3</sup> /kg
電流密度	アンペア毎平方メートル	A/m <sup>2</sup>
磁界の強さ	アンペア毎メートル	A/m
量濃度 <sup>(a)</sup> , 濃度	モル毎立方メートル	mol/m <sup>3</sup>
質量濃度	キログラム毎立方メートル	kg/m <sup>3</sup>
輝度	カンデラ毎平方メートル	cd/m <sup>2</sup>
屈折率 <sup>(b)</sup>	(数字の)	1
比透磁率 <sup>(b)</sup>	(数字の)	1

(a) 量濃度 (amount concentration) は臨床化学の分野では物質濃度 (substance concentration) ともよばれる。  
 (b) これらは無次元量あるいは次元1をもつ量であるが、そのことを表す単位記号である数字の1は通常は表記しない。

表3. 固有の名称と記号で表されるSI組立単位

組立量	SI 組立単位			
	名称	記号	他のSI単位による表し方	SI基本単位による表し方
平面角	ラジアン <sup>(b)</sup>	rad	1 <sup>(b)</sup>	m/m
立体角	ステラジアン <sup>(b)</sup>	sr <sup>(c)</sup>	1 <sup>(b)</sup>	m <sup>2</sup> /m <sup>2</sup>
周波数	ヘルツ <sup>(d)</sup>	Hz		s <sup>-1</sup>
力	ニュートン	N		m kg s <sup>-2</sup>
圧力, 応力	パスカル	Pa	N/m <sup>2</sup>	m <sup>-1</sup> kg s <sup>-2</sup>
エネルギー, 仕事, 熱量	ジュール	J	N m	m <sup>2</sup> kg s <sup>-2</sup>
仕事率, 工率, 放射束	ワット	W	J/s	m <sup>2</sup> kg s <sup>-3</sup>
電荷, 電気量	クーロン	C		s A
電位差 (電圧), 起電力	ボルト	V	W/A	m <sup>2</sup> kg s <sup>-3</sup> A <sup>-1</sup>
静電容量	ファラド	F	C/V	m <sup>2</sup> kg <sup>-1</sup> s <sup>4</sup> A <sup>2</sup>
電気抵抗	オーム	Ω	V/A	m <sup>2</sup> kg s <sup>-3</sup> A <sup>-2</sup>
コンダクタンス	ジーメン	S	A/V	m <sup>2</sup> kg <sup>-1</sup> s <sup>3</sup> A <sup>2</sup>
磁束	ウェーバ	Wb	Vs	m <sup>2</sup> kg s <sup>-2</sup> A <sup>-1</sup>
磁束密度	テスラ	T	Wb/m <sup>2</sup>	kg s <sup>-2</sup> A <sup>-1</sup>
インダクタンス	ヘンリー	H	Wb/A	m <sup>2</sup> kg s <sup>-2</sup> A <sup>-2</sup>
セルシウス温度	セルシウス度 <sup>(e)</sup>	°C		K
光照射量	ルーメン	lm	cd sr <sup>(c)</sup>	cd
放射線量	グレイ	Gy	J/kg	m <sup>2</sup> s <sup>-2</sup>
放射線当量, 周辺線量当量, 方向性線量当量, 個人線量当量	シーベルト <sup>(g)</sup>	Sv	J/kg	m <sup>2</sup> s <sup>-2</sup>
酸素活性	カタール	kat		s <sup>-1</sup> mol

(a) SI接頭語は固有の名称と記号を持つ組立単位と組み合わせても使用できる。しかし接頭語を付した単位はもはやコヒーレントではない。  
 (b) ラジアンとステラジアンは数字の1に対する単位の特別な名称で、量についての情報をつたえるために使われる。実際には、使用する時には記号rad及びsrが用いられるが、習慣として組立単位としての記号である数字の1は明示されない。  
 (c) 測光学ではステラジアンという名称と記号srを単位の表し方の中に、そのまま維持している。  
 (d) ヘルツは周期現象についてのみ、ベクレルは放射性核種の統計的過程についてのみ使用される。  
 (e) セルシウス度はケルビンの特別な名称で、セルシウス温度を表すために使用される。セルシウス度とケルビンの単位の大きさは同一である。したがって、温度差や温度間隔を表す数値はどちらの単位で表しても同じである。  
 (f) 放射性核種の放射能 (activity referred to a radionuclide) は、しばしば誤った用語で"radioactivity"と記される。  
 (g) 単位シーベルト (PV, 2002, 70, 205) についてはCIPM勧告2 (CI-2002) を参照。

表4. 単位の中に固有の名称と記号を含むSI組立単位の例

組立量	SI 組立単位		
	名称	記号	SI 基本単位による表し方
粘力のモーメント	パスカル秒	Pa s	m <sup>-1</sup> kg s <sup>-1</sup>
表面張力	ニュートンメートル	N m	m <sup>2</sup> kg s <sup>-2</sup>
角速度	ニュートン毎メートル	N/m	kg s <sup>-2</sup>
角加速度	ラジアン毎秒	rad/s	m m <sup>-1</sup> s <sup>-1</sup> = s <sup>-1</sup>
熱流密度, 放射照度	ラジアン毎秒毎秒	rad/s <sup>2</sup>	m m <sup>-1</sup> s <sup>-2</sup> = s <sup>-2</sup>
熱容量, エントロピー	ワット毎平方メートル	W/m <sup>2</sup>	kg s <sup>-3</sup>
比熱容量, 比エントロピー	ジュール毎ケルビン	J/K	m <sup>2</sup> kg s <sup>-2</sup> K <sup>-1</sup>
比エネルギー	ジュール毎キログラム毎ケルビン	J/(kg K)	m <sup>2</sup> s <sup>-2</sup> K <sup>-1</sup>
熱伝導率	ジュール毎キログラム	J/kg	m <sup>2</sup> s <sup>-2</sup>
体積エネルギー	ワット毎メートル毎ケルビン	W/(m K)	m kg s <sup>-3</sup> K <sup>-1</sup>
電界の強さ	ジュール毎立方メートル	J/m <sup>3</sup>	m <sup>-1</sup> kg s <sup>-2</sup>
電荷密度	ジュール毎立方メートル	V/m	m kg s <sup>-3</sup> A <sup>-1</sup>
電表面電荷	クーロン毎立方メートル	C/m <sup>3</sup>	m <sup>-3</sup> s A
電束密度, 電気変位	クーロン毎平方メートル	C/m <sup>2</sup>	m <sup>-2</sup> s A
誘電率	クーロン毎平方メートル	C/m <sup>2</sup>	m <sup>2</sup> s A
透磁率	ファラド毎メートル	F/m	m <sup>3</sup> kg <sup>-1</sup> s <sup>4</sup> A <sup>2</sup>
モルエネルギー	ヘンリー毎メートル	H/m	m kg s <sup>-2</sup> A <sup>-2</sup>
モルエントロピー, モル熱容量	ジュール毎モル	J/mol	m <sup>2</sup> kg s <sup>-2</sup> mol <sup>-1</sup>
照射線量 (X線及びγ線)	ジュール毎モル毎ケルビン	J/(mol K)	m <sup>2</sup> kg s <sup>-2</sup> K <sup>-1</sup> mol <sup>-1</sup>
吸収線量率	クーロン毎キログラム	C/kg	kg <sup>-1</sup> s A
放射線強度	グレイ毎秒	Gy/s	m <sup>2</sup> s <sup>-3</sup>
放射輝度	ワット毎ステラジアン	W/sr	m <sup>4</sup> m <sup>-2</sup> kg s <sup>-3</sup> = m <sup>2</sup> kg s <sup>-3</sup>
酵素活性濃度	ワット毎平方メートル毎ステラジアン	W/(m <sup>2</sup> sr)	m <sup>2</sup> m <sup>-2</sup> kg s <sup>-3</sup> = kg s <sup>-3</sup>
	カタール毎立方メートル	kat/m <sup>3</sup>	m <sup>3</sup> s <sup>-1</sup> mol

表5. SI 接頭語

乗数	名称	記号	乗数	名称	記号
10 <sup>24</sup>	ヨタ	Y	10 <sup>1</sup>	デシ	d
10 <sup>21</sup>	ゼタ	Z	10 <sup>2</sup>	センチ	c
10 <sup>18</sup>	エクサ	E	10 <sup>3</sup>	ミリ	m
10 <sup>15</sup>	ペタ	P	10 <sup>6</sup>	マイクロ	μ
10 <sup>12</sup>	テラ	T	10 <sup>9</sup>	ナノ	n
10 <sup>9</sup>	ギガ	G	10 <sup>12</sup>	ピコ	p
10 <sup>6</sup>	メガ	M	10 <sup>15</sup>	フェムト	f
10 <sup>3</sup>	キロ	k	10 <sup>18</sup>	アト	a
10 <sup>2</sup>	ヘクト	h	10 <sup>21</sup>	ゼプト	z
10 <sup>1</sup>	デカ	da	10 <sup>24</sup>	ヨクト	y

表6. SIに属さないが、SIと併用される単位

名称	記号	SI 単位による値
分	min	1 min=60 s
時	h	1 h=60 min=3600 s
日	d	1 d=24 h=86 400 s
度	°	1°=(π/180) rad
分	'	1'=(1/60)°=(π/10 800) rad
秒	"	1"=(1/60)'=(π/648 000) rad
ヘクタール	ha	1 ha=1 hm <sup>2</sup> =10 <sup>4</sup> m <sup>2</sup>
リットル	L, l	1 L=1 l=1 dm <sup>3</sup> =10 <sup>3</sup> cm <sup>3</sup> =10 <sup>-3</sup> m <sup>3</sup>
トン	t	1 t=10 <sup>3</sup> kg

表7. SIに属さないが、SIと併用される単位で、SI単位で表される数値が実験的に得られるもの

名称	記号	SI 単位で表される数値
電子ボルト	eV	1 eV=1.602 176 53(14)×10 <sup>-19</sup> J
ダルトン	Da	1 Da=1.660 538 86(28)×10 <sup>-27</sup> kg
統一原子質量単位	u	1 u=1 Da
天文単位	ua	1 ua=1.495 978 706 91(6)×10 <sup>11</sup> m

表8. SIに属さないが、SIと併用されるその他の単位

名称	記号	SI 単位で表される数値
バール	bar	1 bar=0.1MPa=100 kPa=10 <sup>5</sup> Pa
水銀柱ミリメートル	mmHg	1 mmHg=133.322Pa
オングストローム	Å	1 Å=0.1nm=100pm=10 <sup>-10</sup> m
海里	M	1 M=1852m
バイン	b	1 b=100fm <sup>2</sup> =(10 <sup>12</sup> cm <sup>2</sup> ) <sup>2</sup> =10 <sup>-28</sup> m <sup>2</sup>
ノット	kn	1 kn=(1852/3600)m/s
ネーパ	Np	SI単位との数値的関係は、 対数量の定義に依存。
ベレル	B	
デシベル	dB	

表9. 固有の名称をもつCGS組立単位

名称	記号	SI 単位で表される数値
エルグ	erg	1 erg=10 <sup>-7</sup> J
ダイン	dyn	1 dyn=10 <sup>-5</sup> N
ポアズ	P	1 P=1 dyn s cm <sup>-2</sup> =0.1Pa s
ストークス	St	1 St=1cm <sup>2</sup> s <sup>-1</sup> =10 <sup>-4</sup> m <sup>2</sup> s <sup>-1</sup>
スチルブ	sb	1 sb=1cd cm <sup>-2</sup> =10 <sup>4</sup> cd m <sup>-2</sup>
フオト	ph	1 ph=1cd sr cm <sup>-2</sup> =10 <sup>4</sup> lx
ガリ	Gal	1 Gal=1cm s <sup>-2</sup> =10 <sup>-2</sup> ms <sup>-2</sup>
マクスウェル	Mx	1 Mx=1 G cm <sup>2</sup> =10 <sup>-8</sup> Wb
ガウス	G	1 G=1Mx cm <sup>-2</sup> =10 <sup>-4</sup> T
エルステッド <sup>(a)</sup>	Oe	1 Oe <sub>e</sub> =(10 <sup>3</sup> /4π)A m <sup>-1</sup>

(a) 3元系のCGS単位系とSIでは直接比較できないため、等号「△」は対応関係を示すものである。

表10. SIに属さないその他の単位の例

名称	記号	SI 単位で表される数値
キュリー	Ci	1 Ci=3.7×10 <sup>10</sup> Bq
レントゲン	R	1 R=2.58×10 <sup>-4</sup> C/kg
ラド	rad	1 rad=1cGy=10 <sup>-2</sup> Gy
レム	rem	1 rem=1 cSv=10 <sup>-2</sup> Sv
ガンマ	γ	1 γ=1 nT=10 <sup>-9</sup> T
フェルミ	f	1 フェルミ=1 fm=10 <sup>-15</sup> m
メートル系カラット		1 メートル系カラット=0.2 g=2×10 <sup>-4</sup> kg
トル	Torr	1 Torr=(101 325/760) Pa
標準大気圧	atm	1 atm=101 325 Pa
カロリ	cal	1 cal=4.1858J (「15°C」カロリ), 4.1868J (「IT」カロリ), 4.184J (「熱化学」カロリ)
マイクロン	μ	1 μ=1μm=10 <sup>-6</sup> m

